(NASA-CR-169084) MEASUREMENTS OF DISPLACEMENT AROUND HOLES IN COMPOSITE PLATES SUBJECTED TO QUASI-STATIC COMPRESSION Final Report, 1 Jun. - 31 May 1982 (Virginia Polytechnic Inst. and State Univ.) 57 p G3/39

N82-26712

Unclas 28165

Measurement of Displacement Around Holes in Composite Plates Subjected to Quasi-Static Compression

Final Report of Work under NAG-1-193
June 1, 1982 - May 31, 1982

John C. Duke, Jr.,* Daniel Post,* Robert Czarnek,**
and Anand Asundi***

Engineering Science and Mechanics Department
Virginia Polytechnic Institute and State University
Blackskburg, VA 24061

* Principal Investigators
** Graduate Student
*** Post-doctoral Research Associate

DTIC DOES NOT HAVE THIS ITEM

-- 1 - AD NUMBER: D436327
-- 5 - CORPORATE AUTHOR: VIRGINIA POLYTECHNIC INST AND STATE UNIV
-- BLACKSBURG DEPT OF ENGINEERING SCIENCE AND MECHANICS
-- 6 - UNCLASSIFIED TITLE: MEASUREMENT OF DISPLACEMENT AROUND HOLES IN
-- COMPOSITE PLATES SUBJECTED TO QUASI-STATIC COMPRESSION.
-- 9 - DESCRIPTIVE NOTE: FI REPT; 1 JUN 81-31 MAY 82
--10 - PERSONAL AUTHORS: DUKE,J. C. , JR.;POST,D. ;CZARNEK,R. ;ASUNDI,A. ;
--12 - PAGINATION: 57P
--15 - CONTRACT NUMBER: NAG-1-193
--18 - MONITOR ACRONYM: NASA
--19 - MONITOR SERIES: CR-169084
--20 - REPORT CLASSIFICATION: UNCLASSIFIED
--22 - LIMITATIONS (ALPHA): APPROVED FOR PUBLIC RELEASE; DISTRIBUTION
-- UNLIMITED. AVAILABILITY: NATIONAL TECHNICAL INFORMATION SERVICE,
-- SPRINGFIELD, VA. 22161. N82-26712.
--33 - LIMITATION CODES: 1 24

Preface

This is the final report of work supported by the National Aeronautics and Space Administration Langley Research Center under Research Grant No. NAG-1-193. The technical officer has been Dr. James H. Starnes, Jr. and the Grants Officer Mr. C. L. Crowder, Jr.

Table of Contents

INTRODUCTION

This study is part of a continuing exploration of the structural behavior of fiber-reinforced composite materials by NASA (Langley). The dual purposes of the present research are to

(1) develop a whole-field, high-sensitivity optical technique to measure load-induced changes of thickness of composite plates, and

(2) measure changes of thickness of three composite plates, each with a central hole of different prescribed size, as a function of applied compressive loads.

The specimens were graphite-epoxy plates of quasi-isotropic layup, having dimensions shown in Fig. 1, and all presumably cut from the same larger plate. They were supplied by NASA.

OPTICAL METHOD

Basic Approach

When external loads are applied to a plate, its thickness changes and its surfaces experience out-of-plane displacements W_I and W_{II}, as illustrated in Fig. 2. In general these changes vary across the plate as a function of x and y.

In the scheme developed here for thickness change measurements, a variation of holographic interferometry is used first to produce whole-field contour maps of W_I and W_{II}. Its sensitivity is $\lambda/2$ displacement per fringe order (or contour level) of the contour map. At any point x, y in the specimen,

$$W_I = \frac{\lambda}{2} N_I \quad ; \quad W_{II} = \frac{\lambda}{2} N_{II} \tag{1}$$

where λ is the wavelength used to construct the hologram and

N_I, N_{II} are fringe orders at that point in the reconstructed holographic interferometry patterns from faces I and II, respectively.

Of course, the total thickness change, ΔT, at any point x, y is

$$\Delta T = W_I + W_{II} = \frac{\lambda}{2} (N_I + N_{II}) \tag{2}$$

The method would be most effective if the patterns from the two faces are combined into a single contour map of ΔT. While it is better known that contour maps can be subtracted by moire methods, moire can be used to add contour maps, too.

In the present method, carrier patterns of equal frequencies and opposite signs are added to the fringe patterns. Fringe orders at any point x, y are thereby changed to $N_I + N_C$ and $N_{II} - N_C$, where N_C represents the fringe order attributable to the carrier pattern. When these two contour maps are superimposed they interweave to form a moire pattern of the additive parameter, N, where

$$N = (N_I + N_C) + (N_{II} - N_C) = N_I + N_{II} \tag{3}$$

Equations (2) and (3) combine to show that the moire fringe order at each point x, y is proportional to the thickness change at that point by

$$\Delta T = \frac{\lambda}{2} N \qquad (4)$$

Optical filtering is used to enhance contrast of the moire pattern, thus producing a clear contour map of thickness changes throughout the field of view.

The final contour map gives relative values of ΔT, however, and it is necessary to know the absolute value of ΔT at some point in the field of view to assign absolute values throughout the field. This is accomplished by a rather simple optical clip gage attached to the specimen.

Whereas holographic interferometry is usually conducted with specimens that produce matte (or diffuse) reflection of light, [1, 2] the specimens used in this study were prepared with smooth, specularly reflecting faces. Accordingly, the problems associated with speckles, including speckle correlation and loss of fringe contrast, encountered with matte surfaces in holographic interferometry were circumvented.

The optical method is described in greater detail in the following sections. To the best of our knowledge, it is original.

EXPERIMENTAL PROCEDURE

Nondestructive Examination

Upon receipt of the specimens each was examined nondestructively by pulse echo ultrasonic C-scanning. The amplitude of the backsurface echo from each specimen was recorded and reproduced as Figs. 3-5. Regions which appear white in the C-scan plots correspond to places in the specimens where the amplitude was significantly lower than regions which appear black. The quality of the three specimens appears to be typical.

Specimen Preparation

The specimens were prepared with smooth mirrorized coatings. First, a thin layer of room-temperature curing epoxy was cast on each face, using the smooth surface of a thin Plexiglas plate as an external mold. Ultra-thin aluminum was coated on the smooth epoxy by vacuum deposition. Reference lines were scribed at corresponding locations on the two faces.

Loading

Each specimen was loaded in compression, using a NASA fixture to engage its perimeter and prevent gross buckling. A Tinius Olsen testing machine of 120,000 pounds capacity was used. A spherical seat on the upper loading anvil was adjusted to produce nearly uniform loading across the width and thickness of the specimen, as indicated by four electric strain gages on the specimen (Fig. 1). The adjustment was made at approximately 15,000 pounds compressive load and it was maintained by friction in the spherical seat for the remainder of the test. The load was reduced to about 500 pounds to begin the test sequence.

Holograms were made for load increments of approximately 15,000 pounds up to about 70% of maximum load. Then, increments were reduced gradually to 3000 pounds near anticipated failure of the specimen. Strain gage data was taken for each load increment to assess load uniformity.

Hologram Exposures

The basic experimental data was obtained by reflection-type holographic interferometry. For this, the fixture shown in Fig. 6 was used to hold a high resolution photographic plate adjacent to each mirrorized surface of the

specimen. The specimen and photographic plates were illuminated from each side by the dual optical system illustrated in Fig. 7a. Light from the expanded and collimated laser beam passed through the photographic emulsion (Fig. 7b), reflected back from the specimen surface, and penetrated the emulsion again. Thus, the emulsion was exposed simultaneously to two coherent beams with wavefronts WF_1 and WF_2, which interacted to produce a stationary pattern of interference fringes. The beam with WF_1 is the reference beam while that with WF_2 is the information beam.

The fringes lie along the bisector of the wavefronts, forming adjacent planes or walls of constructive and destructive interference nearly parallel to the specimen surface. About 60 such walls are produced within the small thickness (approximately 13 microns) of the emulsion.

A double exposure is made for each load increment. After the first exposure,

(1) The photographic plates are inclined through an identical small angle to create the carrier pattern. This is done by advancing the micrometer screw on the holographic plate fixture (Fig. 6). Then
(2) the specimen is loaded in compression to a predetermined load, and
(3) the second holographic exposures are made on the same photographic plates.

These exposures are made in a dark enclosure--a light-tight polyethelene enclosure built around the testing machine. After each load increment, the photographic plates are removed, fresh plates are installed and the steps are repeated for another increment of compressive load, with the sequence continuing until the breaking load is reached.

Reconstruction

Each photographic plate contains two interweaving systems of interference, as illustrated with exaggerated angles in Fig. 8. The light reflecting back from the surface of the specimen does not have a plane wavefront, but instead it has a warped wavefront with warpage twice that of the mirrorized specimen surface. Consequently, the walls of constructive interference are warped in harmony with the specimen warpage. The photographic plate--now called a hologram--contains complete information on the out-of-plane warpage of the specimen before and after the load increment. In addition, this information is separated by the small ($\approx 1/3^0$) constant angle introduced between exposures.

After development, the photographic emulsion is comprised of partially transparent walls of silver in the zones of constructive interference, separated by clear walls of gelatin lying in the zones of destructive interference. These silver walls act as partial mirrors--internal mirrors in the volume of the emulsion. Upon reconstruction, light is reflected at the successive mirrors as shown for only one system at the top of Fig. 9. The optical path length between these adjacent mirror walls is half a wavelength, so each emergent contribution is one wavelength out-of-phase with its neighbors. The result is constructive interference between all these contributions, producing a reasonably strong reflection.

Three beams emerge from the hologram: a beam from the glass/emulsion interface (and glass/air interface), which is wasted; and two beams from the internal mirrors which carry the desired information and are collected by the observer.

The optical system for reconstruction is illustrated in Fig. 10. A convergent beam of laser light illuminates the hologram through action of a

beam-splitter. The two information beams converge to small zones in the plane of the camera aperture and they are admitted into the camera. The third beam from the hologram surface emerges in a different direction and it is stopped by the aperture; note that this is the reason for the inclination of the photographic plate shown in Figs. 7-9. The two information beams that reflect from the internal mirrors of the hologram have warped wavefronts and the camera photographs the interference pattern generated by interaction of these two coherent beams.

The interference pattern is a contour map of the separation or gap, s, between the wavefronts (in the object plane or specimen plane of the hologram). This is illustrated schematically and greatly exaggerated in Fig. 11a, where the two wavefronts have different shapes since they represent different states of specimen deformation. Furthermore, the two wavefronts exhibit a general inclination with respect to each other (shown by dashed lines), corresponding to the change of inclination of the holographic plate introduced between the exposures.

If the two wavefronts had identical warpage, the contour map of s would be parallel equally spaced fringes induced by the inclination alone. This uniform fringe gradient is called a carrier pattern. In the actual event, information depicting the difference of warpage of the two wavefronts is introduced as variations in the otherwise regular carrier pattern, as sketched in Fig. 11b.

Accordingly, at any specimen point x, y, the fringe order M in Fig. 11b is the sum of the fringe orders attributable to the wavefront warpage and the carrier pattern. For face I this is

$$M_I = N_I + N_{cI} \tag{5}$$

$$M_I = N_I + N_{cI} \tag{5}$$

and for face II

$$M_{II} = N_{II} + N_{cII} \tag{6}$$

Alternative Explanation

In the argument presented here, the wavefronts of light emerging from the hologram in the reconstruction step are identical to those striking the photographic plate in the hologram construction step. However, this does not account for the fact that the emulsion of the photographic plate shrinks in thickness as a result of processing. After processing, the distance between internal mirrors (Fig. 9) is less than the distance between walls of constructive interference of the exposure (Fig. 7). Thus, constructive interference of contributions from each partial mirror occurs for a shorter wavelength. At the same time, warpage of the internal mirrors is diminished uniformly across the hologram by the same proportion. As a result, the wavefront warpage will produce exactly the same interference pattern with the shorter wavelength as an unshrunken hologram would produce with the original wavelength.

This suggests that precisely the right shorter wavelength must be used to obtain a correct pattern of W displacements. In practice, however, the contour map produced by reconstruction is unique, while its intensity is influenced by the wavelength of reconstruction. The following alternative explanation of reconstruction supports this.

Consider the zone near AA in Fig. 8. Walls of constructive interference from exposures 1 and 2 are superimposed; after development, successive partial mirrors of silver reflect light in the reconstruction process. Along BB, however, the walls of constructive interference of exposure 2 fall exactly

between those of exposure 1. Since the intensities of the individual interference patterns are harmonic, the two intensities with a half-cycle shift sum to a constant value across BB. Near BB there are no partial mirror surfaces and no directed light reflects from the interior of the emulsion. The positions of these zones of reflectivity (AA) and non-reflectivity (BB) correspond to the positions of constructive and destructive interference viewed in the camera. Since emulsion shrinkage does not alter the positions of zones AA and BB, the resultant pattern is independent of shrinkage.

In this work, red light of helium-neon lasers (λ = 24.9 μin or 633 nm) was used to produce the holograms. After processing, reflection of green light was strongest and green light of an argon laser (λ = 20.2 μin or 514 nm) was used for reconstruction.

Summation by Moire and Optical Filtering

Two films with patterns corresponding to Fig. 11b are produced by reconstruction, one from each side of the specimen. Their superposition produces a moire pattern and, in order to support Eqs. (3) and (4), it remains to show that this is a pattern of $N_I + N_{II}$.

Let the y-axis correspond to the axis of rotation of the fixture carrying the two holographic plates (Fig. 2). With this linkage, the change of gap between specimen and hologram, caused by rotation of the fixture, is exactly equal and opposite for every corresponding point x, y on Faces I and II. Therefore, fringe orders attributable to the carrier pattern are exactly opposite and Eqs. (5) and (6) may be written

$$M_I = N_I + N_c \quad ; \quad M_{II} = N_{II} - N_c \qquad (7)$$

It is well established [3] that superposition of two contour maps with contours of M_I and M_{II} produces a moire pattern in which the subtractive parameter $M_{II} - M_I$ and the additive parameter $M_{II} + M_I$ are both present. Only one of the two parameters emerges with good visibility.

In the present case, superposition of the two reconstructed holograms, namely, superposition of contours M_I and M_{II}, produces the subtractive moire

$$M_{II} - M_I = N_{II} - N_I - 2N_c \tag{8}$$

and the additive moire

$$M_{II} + M_I = N_{II} + N_I \tag{9}$$

Since the carrier pattern is adjusted to dominate, N_c is large compared to $N_{II} - N_I$; the subtractive moire has very closely spaced fringes, with the general appearance of Fig. 11b. The additive moire has relatively few fringes across the field of view, and these moire fringes appear with good visibility on a background of the subtractive moire field. In this case, because carrier patterns of opposite signs were used, superposition yields the additive moire of Eq. (9).

When the films from hologram reconstructions of Faces I and II are superimposed, the moire fringes have the general appearance shown in Fig. 12a. Broad zones of continuous black areas are formed where dark and light bands interweave. Elsewhere, striped zones remain.

Figure 12b illustrates a simple means of further enhancing contrast of the additive moire pattern by optical filtering. When the superimposed films are inserted into this arrangement, the striped zones diffract light into many diffraction orders. The camera aperture is adjusted to accept light from the first diffraction order only, thus projecting uniform bright bands of light into the image plane from the striped zones on the object.

Sensitivity

By Eq. 4, the sensitivity is $\lambda/2$ change of thickness per fringe order, in the final moire pattern, where λ is the wavelength used to produce the hologram. Here, λ is 24.9 μin (633 nm) and the sensitivity is 12.5 μin (317 nm) per fringe order. The load-induced change of specimen thickness is constant along a continuous fringe, and its magnitude changes by 12.5 μin in the zone between neighboring fringes.

Absolute Thickness Change

While the pattern of N is a contour map of thickness change, it does not necessarily reveal the absolute value of N at any point. For complete information, the absolute value of N at some point must be known from subsidiary information. In many cases it is known from the geometry of the specimen; an example is the case of a specimen with an unloaded external corner, where the stresses are all zero and $\Delta T = N = 0$. In the present case, however, it was necessary to measure the absolute value of ΔT at one point in the field to establish the absolute value of N throughout the field. An optical clip gage was used for the purpose.

Optical Clip Gage*

Optical clip gage 2 is illustrated in Fig. 13. It consists of a rigid spacer cemented to flexible arms on each side of the specimen. The end of each arm is cemented to the specimen as shown and responds to the thickness change of the specimen at the narrow zone of attachment.

---

*Suggested by creative graduate student Robert Czarnek

change of the specimen at the narrow zone of attachment.

The arms have flat mirrorized surfaces like the specimen. These surfaces appear in the field of view of the hologram and changes of gap between the arms and photographic plates are recorded as fringes in the reconstructed hologram. When the two reconstructed holograms are superimposed, the additive moire in the area of the clip gage produces fringes of relative displacement of the two arms, as seen in Fig. 16.

Fringe order at the rigid spacer is zero and the fringe count proceeds monotonically to the fringe order at the cemented portion. Here, the thickness change in the specimen is equal to the relative displacement of the arms. Therefore, the fringe passing through this zone in the specimen pattern has the same fringe order as the clip gage. This establishes a starting point for the fringe count in the specimen.

EXPERIMENTAL RESULTS

The results of the three tests performed in this study are presented in chronological order of their performance. For each hologram, the load levels and associated strain gage readings are presented in tabular form in Tables 1-3. Following each table are photographs of the contour maps associated with the indicated load increment. Figures 14 and 15 display contour maps for the specimen with the 1/2 inch hole; Figs. 16 and 17 show contour maps for the specimen with the 3/4 inch hole; and Fig. 18 and 19 shows contour maps for the specimen with the 1/4 inch hole. Certain maps are not presented and the explanation of their absence is given in the section entitled Discussion of Results. The contour maps for the specimen containing the 3/4 inch hole have been interpreted. The change in thickness along the boundary of the hole,

which has occurred as a result of the second increment of load, is presented as a polar plot in Fig. 20. The accumulated thickness changes that occurred at the horizontal midplane are presented in Fig. 21.

Calculation of Change in Thickness at a Point

The following procedure was followed to calculate the absolute change in thickness at any point in the field of view. For each pattern, the fringe order in the clip gage at its zone of attachment was counted, assuming zero order at the center of the rigid spacer. The contour line of specimen thickness that passed through the zone of attachment was assigned the same fringe order. Then, the surrounding fringes were enumerated by the rules of topography and casual knowledge of the nature of deformation for such a specimen. The resulting fringe orders are given in Figs. 14 and 15 for the specimen with the 3/4 inch hole.

At any given point, the total change of thickness after the i^{th} load increment is given by

$$\Delta T_i = (N_1 + N_2 + \text{---} + N_i)\,\frac{\lambda}{2} \qquad (10)$$

where N_1, N_2, ---, represent fringe orders at the given point for each step of the loading sequence. The accumulated thickness changes shown in Fig. 21 were determined by this procedure.

DISCUSSION OF RESULTS

The test results have been presented chronologically so that an explanation of changes in procedure might be recognized.

The specimen with the 1/2 inch plate was the first tested, and the clip gage employed there did not function properly. This was unexpected, since preliminary tests indicated it should be dependable. The gage arms did not behave as rigid bodies as required, but instead, the change in thickness patterns show deformation of the arms. The original clip gage design was abandoned and the gage design of Fig. 13 was subsequently used.

Contour maps from this first test (1/2 inch hole) showed zones where no fringes were present, surrounded by zones of low fringe contrast. No optical explanation seemed plausable and since holographic exposures were made very soon after load application, it was thought to result from localized motion or creep of the specimen during the period of holographic exposure (about 10 seconds). If the specimen surface moves in the W direction by 1/4 of a wavelength, or 6 μin, constructive interference on the hologram changes to destructive interference and destroys the fringes of the hologram. We cannot say with certainty that this is the explanation, particularly since only small portions of the field were involved, whereas creep might be expected to be more widespread. A minimum interval of 5 minutes was used in subsequent tests between specimen loading and the holographic exposures; localized zones of absent fringes were not found in subsequent tests. The next test, using the specimen with the 3/4 inch hole, was superbly successful--except for one blunder. A fringe pattern for the first load increment, 500 to 15,000 pounds, is not shown, and this is because one of the holographic exposures was absent. Apparently, a protective shield was not withdrawn and it blocked the light intended to expose the hologram. Such a blunder can be avoided.

An inexplicable issue manifests itself as radical differences in the quality of fringe patterns. An example is Fig. 18c [1/4 inch hole, load increment #4] which shows excellent quality. Yet, the patterns in the same

sequence for load increments #3, 5 and 6, which were made under identical circumstances, had such poor quality that they are not presented here. Fringes appeared in only a few small zones in the field of view, and even those fringes had low contrast. The same was true for the second load increment with the 1/2 inch hole. No plausable explanation has come forth; even specimen creep seems implausable. What is known, however, is that the quality of the mirror coatings for the specimen with the 3/4 inch hole was superior to those of the other specimens. The results support confidence that excellent change of thickness patterns can be obtained when specimens with excellent mirrorized surfaces are used.

Several interesting features have been observed. First, the fringes in regions of compression are considerably more irregular than those in regions of tension (that occur immediately above and below the hole). It is speculated that local material instabilities, or localized buckling, cause these irregularities. Secondly, although certain aspects of the contour maps appear in general agreement with analyses for isotropic materials--particularly the location of the zero order fringe and the shapes of fringes above and below the hole--others are clearly different. The most prominent difference is the change in thickness along the horizontal midplane. Finally, macroscopic damage appeared prior to failure at positions on either side of the hole above and below the horizontal midplane and increased in extent toward the midplane as the load was increased.

Future Work

The tests were remarkably successful in some ways, yet frustrating in others. Additional experience is required to make the test method fully predictable and routine. A review of this work suggests extensions of special interest as follows.

Full Specimen Width

Thickness changes across the full specimen width could be observed. This would require that the anti-buckling restraint fixture be abandoned, which would restrict the observations to low levels of load.

Warpage of Specimen Surface

While thickness changes remain orderly, the specimen may become severely warped under compressive loading. It would be possible to withdraw contour maps of change of surface warpage from the same holograms used for change of thickness determinations. Out-of-plane displacements are likely to be large compared to the holographic sensitivity of half a wavelength per fringe order and therefore the changes of surface warpage should be evaluated for small increments of load.

REFERENCES

1. C. M. Vest, Holographic Interferometry, John Wiley & Sons, New York (1979).

2. D. B. Newmann and R. C. Penn, "Off-table Holography," Experimental Mechanics, Vol. No. 6, pp. 241-244 (June 1975).

3. A. J. Durelli and V. J. Parks, Moire Analysis of Strain, Prentice-Hall, Inc., Englewood Cliffs, NJ (1970).

TABLE 1
Specimen with 1/2 inch hole
Specimen thickness 0.265 in.

Preliminary Adjustment of Load Axiality was performed at 15,000 lbs.

Hologram Pair No. I Initial Load - 500 lbs. Clock Time - 1:40

Exposure[a]	Clock Time	Load(lbs)	Strain Gage Readings[b] RF	RR	LF	LR
1	1:56	480	68	21	76	75
2	2:00	16000	1267	1217	1197	1246

Hologram Pair No. II Initial Load - 16000 lbs Clock Time - 2:00

Exposure	Clock Time	Load(lbs)	Strain Gage Readings RF	RR	LF	LR
1	2:06	15750	1257	1209	1185	1238
2	2:09	29950	2380	2310	2270	2330

Hologram Pair No. III Initial Load - 29950 lbs Clock Time - 2:09

Exposure	Clock Time	Load(lbs)	Strain Gage Readings RF	RR	LF	LR
1	2:15	29800	2370	2300	2260	2320
2	2:17	45000	3600	3530	3430	3510

Hologram Pair No. IV Initial Load - 45000 lbs Clock Time - 2:17

Exposure	Clock Time	Load(lbs)	Strain Gage Readings RF	RR	LF	LR
1	2:22	44800	3600	3530	3430	3500
2	2:27	57150	4650	4570	4380	4480

Hologram Pair No. V Initial Load - 57150 lbs Clock Time - 2:27

Exposure	Clock Time	Load(lbs)	Strain Gage Readings RF	RR	LF	LR
1	2:32	56900	4640	4570	4370	4470
2	2:35	62050	5080	5000	4760	4880

Note: Damage visible at 4 points around the hole

(a) The inclination of the photographic plates is adjusted before and after each exposure by $+\theta$ and $-\theta$ respectively.
(b) These readings are of axial strain corresponding to a reduction in length in arbitrary units. RF - right front, RR - right rear, LF - left front, LR - left rear.

Table 1 (continued)

Hologram Pair No. VI Initial Load - 62050 lbs Clock Time - 2:35

Exposure	Clock Time	Load(lbs)	Strain Gage Readings RF	RR	LF	LR
1	2:39	62000	5080	5010	4760	4870
2	2:40	65000	5330	5260	4990	5110

Hologram Pair No. VII Initial Load - 65000 lbs Clock Time - 2:40

Exposure	Clock Time	Load(lbs)	Strain Gage Readings RF	RR	LF	LR
1	2:48	64700	5330	5260	4980	5100
2	2:52	68000	5620	5560	5230	5360

Note: Puckering observed adjacent to hole from approximately 45° above to 45° below the horizontal midplane

Hologram Pair No. VIII Initial Load - 68000 lbs Clock Time - 2:52

Exposure	Clock Time	Load(lbs)	Strain Gage Readings RF	RR	LF	LR
1	2:57	67850	5620	5540	5220	5350

Gross failure occurred prior to 71000 lbs and destroyed the photographic plates!

TABLE 2
Specimen with 3/4 inch hole
Specimen thickness 0.265 in.

Preliminary adjustment of load axiality was performed at 15000 lbs.

Hologram Pair No. I Initial Load - 600 lbs Clock time - 1:23

Exposure[a]	Clock Time	Load(lbs)	Strain Gage Readings[b] RF	RR	LF	LR
1	1:53	600	60	+3	115	86
2	2:02	14900	1149	1169	1120	1165

Hologram Pair No. II Initial Load - 15150 lbs Clock Time - 1:57

Exposure	Clock Time	Load(lbs)	Strain Gage Readings RF	RR	LF	LR
1	2:06	14900	1148	1167	1119	1168
2	2:13	29850	2348	2355	2250	2354

Hologram Pair No. III Initial Load - 30050 lbs Clock Time - 2:08

Exposure	Clock Time	Load(lbs)	Strain Gage Readings RF	RR	LF	LR
1	2:18	29850	2345	2356	2250	2354
2	2:26	44650	3583	3598	3368	3535

Hologram Pair No. IV Initial Load - 45000 lbs Clock Time - 2:20

Exposure	Clock Time	Load(lbs)	Strain Gage Readings RF	RR	LF	LR
1	2:31	44550	3582	3597	3368	3534
2	2:37	49925	4046	4065	3777	3973

Hologram Pair No. V Initial Load - 50100 lbs Clock Time - 2:32

Exposure	Clock Time	Load(lbs)	Strain Gage Readings RF	RR	LF	LR
1	2:42	49925	4040	4060	3769	3962
2	2:49	52750	4290	4314	3988	4198

(a) The inclination of the photographic plates is adjusted before and after each exposure by $+\theta$ and $-\theta$ respectively.
(b) These readings are of axial strain corresponding to a reduction in length in arbitrary units. RF - right front, RR - right rear, LF - left front, LR - left rear.

Table 2 (continued)

Hologram Pair No. VI Initial Load - 53000 lbs Clock Time - 2:44

Exposure	Clock Time	Load(lbs)	Strain Gage Readings RF	RR	LF	LR
1	2:54	52750	4288	4312	3985	4194
2	3:00	55800	4567	4593	4222	4445

Hologram Pair No. VII Initial Load - 56000 lbs Clock Time - 2:56

Exposure	Clock Time	Load(lbs)	Strain Gage Readings RF	RR	LF	LR
1	3:06	55800	4562	4590	4216	4439
2	3:16	58850	4846	4874	4457	4699

Hologram Pair No. VIII Initial Load - 59000 lbs Clock Time - 3:08

Exposure	Clock Time	Load(lbs)	Strain Gage Readings RF	RR	LF	LR
1	3:18	58850	4839	4866	4453	4693
2	Gross failure occurred at 62000 lbs and destroyed the photographic plates!					

TABLE 3
Specimen with 1/4 inch hole
Specimen thickness 0.264 in.

Preliminary adjustment of load axiality was performed at 15000 lbs

Hologram Pair No. I Initial Load - 500 lbs Clock Time - 10:30

Exposure[a]	Clock Time	Load(lbs)	Strain Gage Readings[b] RF	RR	LF	LR
1	10:42	550	78	33	103	102
2	10:51	14800	1184	1125	1158	1177

Hologram Pair No. II Initial Load - 15000 lbs Clock Time - 10:46

Exposure	Clock Time	Load(lbs)	Strain Gage Readings RF	RR	LF	LR
1	10:55	14800	1174	1118	1149	1169
2	11:02	29650	2420	2316	2312	2341

Hologram Pair No. III Initial Load - 30000 Clock Time - 10:57

Exposure	Clock Time	Load(lbs)	Strain Gage Readings RF	RR	LF	LR
1	11:06	29650	2414	2312	2305	2334
2	11:14	45250	3787	3643	3536	3593

Hologram Pair No. IV Initial Load - 45600 lbs Clock Time - 11:09

Exposure	Clock Time	Load(lbs)	Strain Gage Readings RF	RR	LF	LR
1	11:18	45250	3777	3635	3527	3585
2	11:25	59400	5110	4924	4639	4729

Hologram Pair No. V Initial Load - 60000 lbs Clock Time - 11:20

Exposure	Clock Time	Load(lbs)	Strain Gage Readings RF	RR	LF	LR
1	11:30	59400	5102	4916	4627	4719
2	11:37	71750	6410	6168	5539	5662

(a) The inclination of the photographic plates is adjusted before and after each exposure by $+\theta$ and $-\theta$ respectively.
(b) These readings are of axial strain corresponding to a reduction in length in arbitrary units. RF - right front, RR - right rear, LF - left front, LR - left rear.

Table 3 (continued)

Hologram Pair No. VI Initial Load - 72100 lbs Clock Time - 11:32

Exposure	Clock Time	Load(lbs)	Strain Gage Readings RF	RR	LF	LR
1	11:43	71650	6407	6163	5528	5651
2	11:50	74750	6794	6536	5721	5858

Hologram Pair No. VII Initial Load - 75000 lbs Clock Time - 11:45

Exposure	Clock Time	Load(lbs)	Strain Gage Readings RF	RR	LF	LR
1	11:54	74750	6793	6534	5712	5847
2	Gross failure occurred at 78000 lbs and destroyed the photographic plates!					

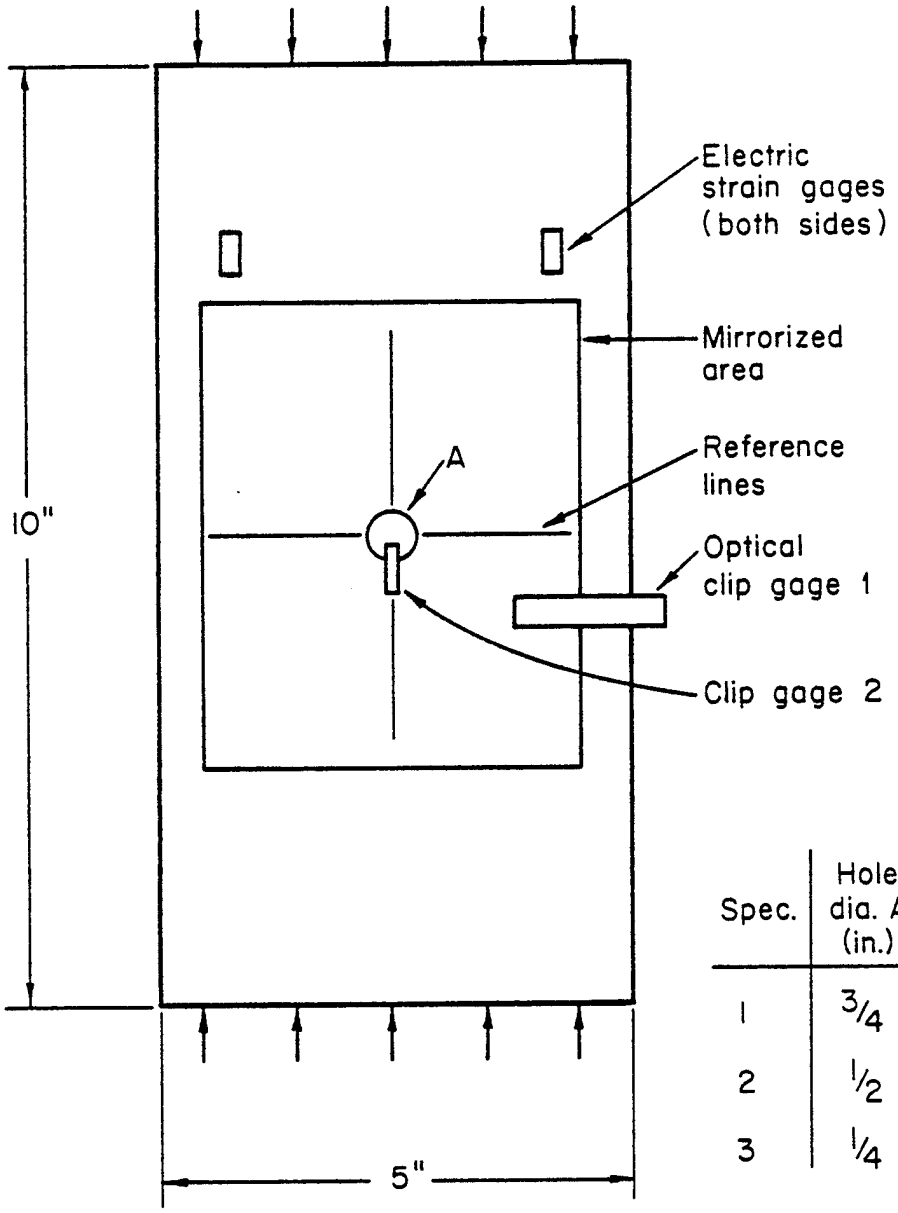

Spec.	Hole dia. A (in.)	Thickness (in.)
1	3/4	0.265
2	1/2	0.265
3	1/4	0.264

Fig. 1. Graphite-epoxy composite specimens for compression tests.

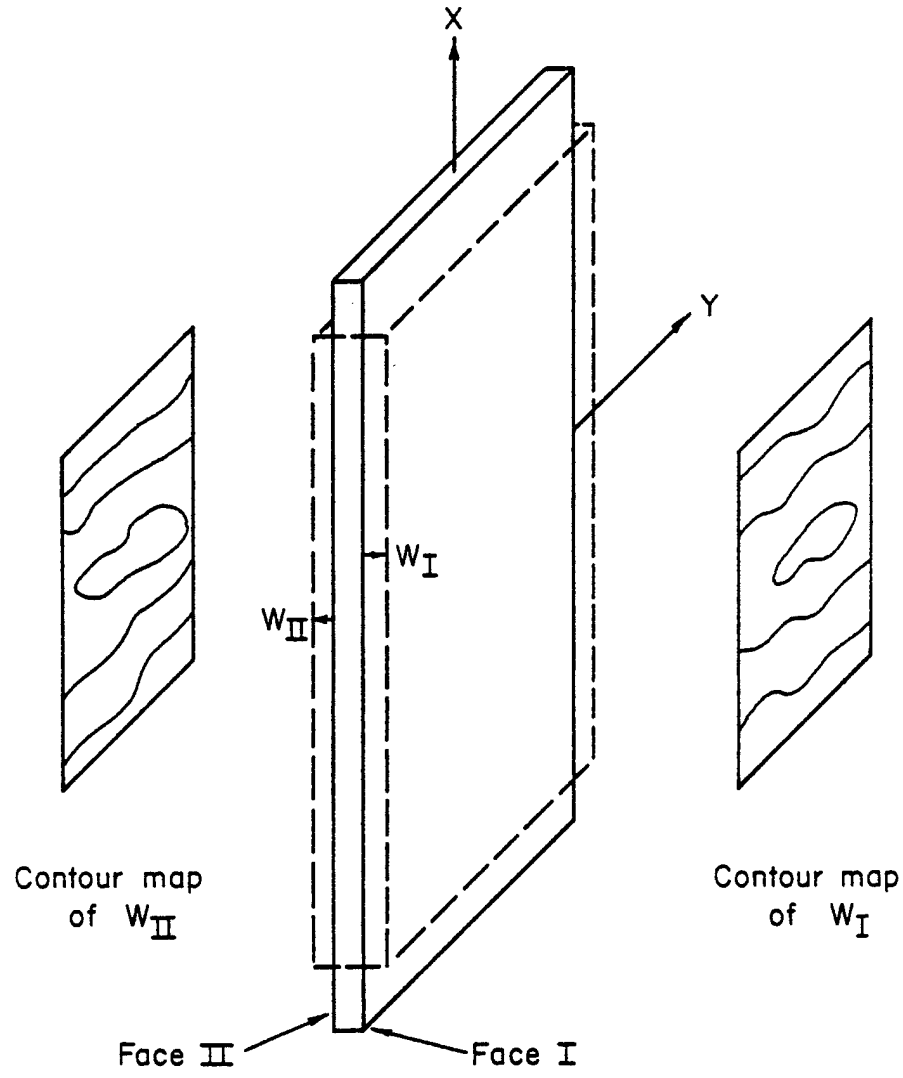

Fig. 2. Out-of-plane displacements of specimen surfaces, shown greatly exaggerated.

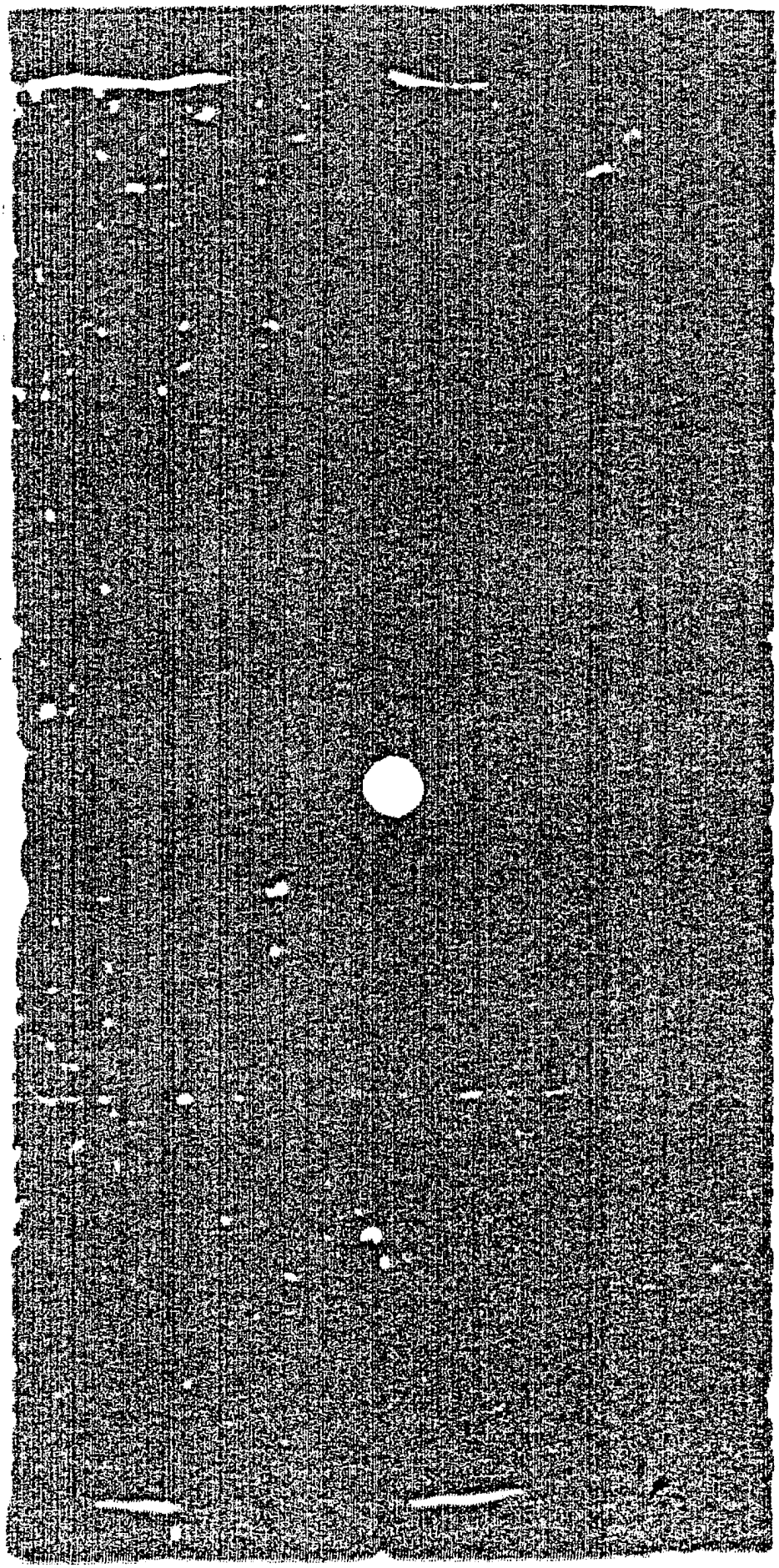

Fig. 3. Ultrasonic C-scan of the test specimen containing a 1/4 inch hole.

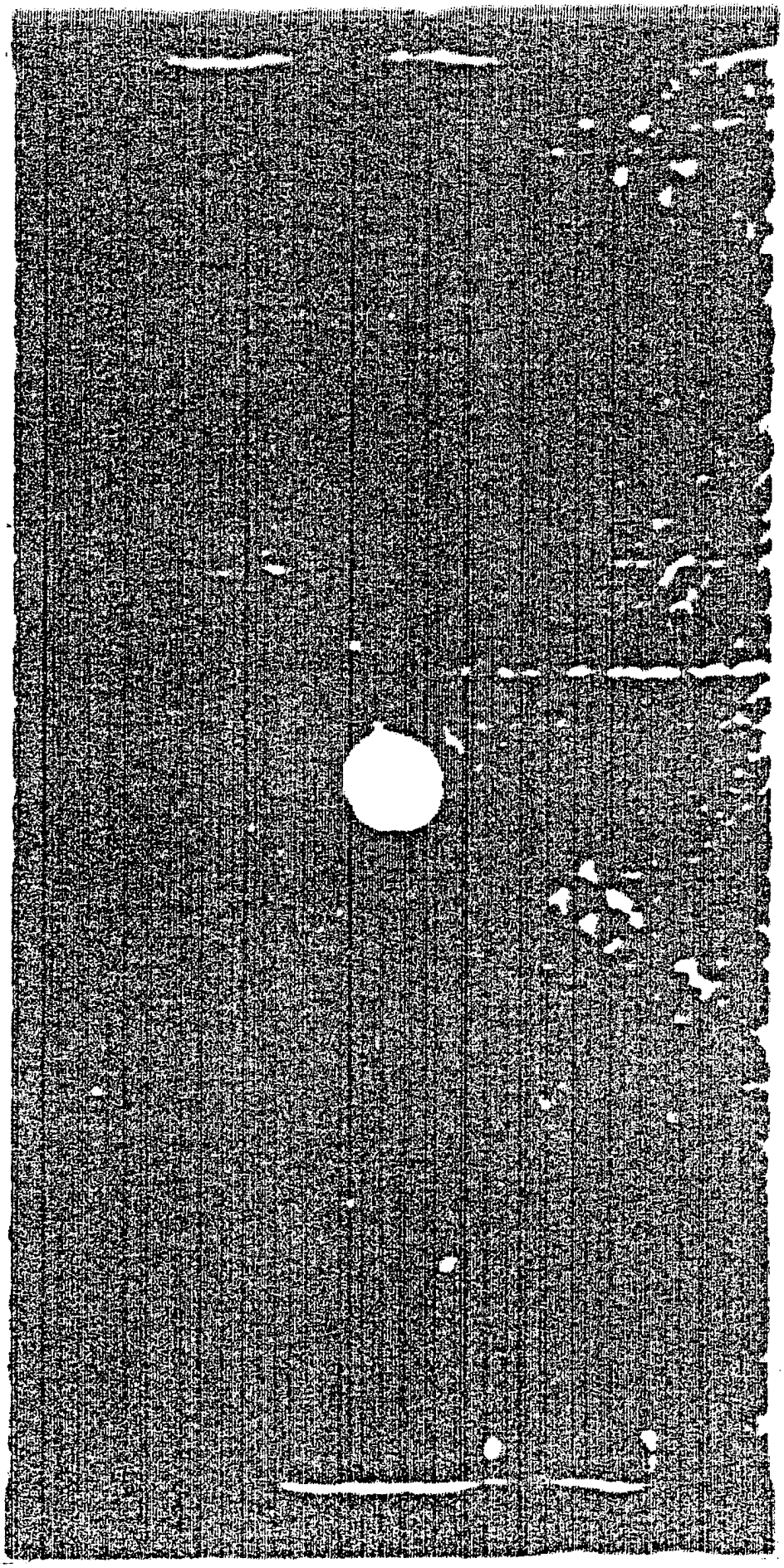

Fig. 4. Ultrasonic C-scan of the test specimen containing a 1/2 inch hole.

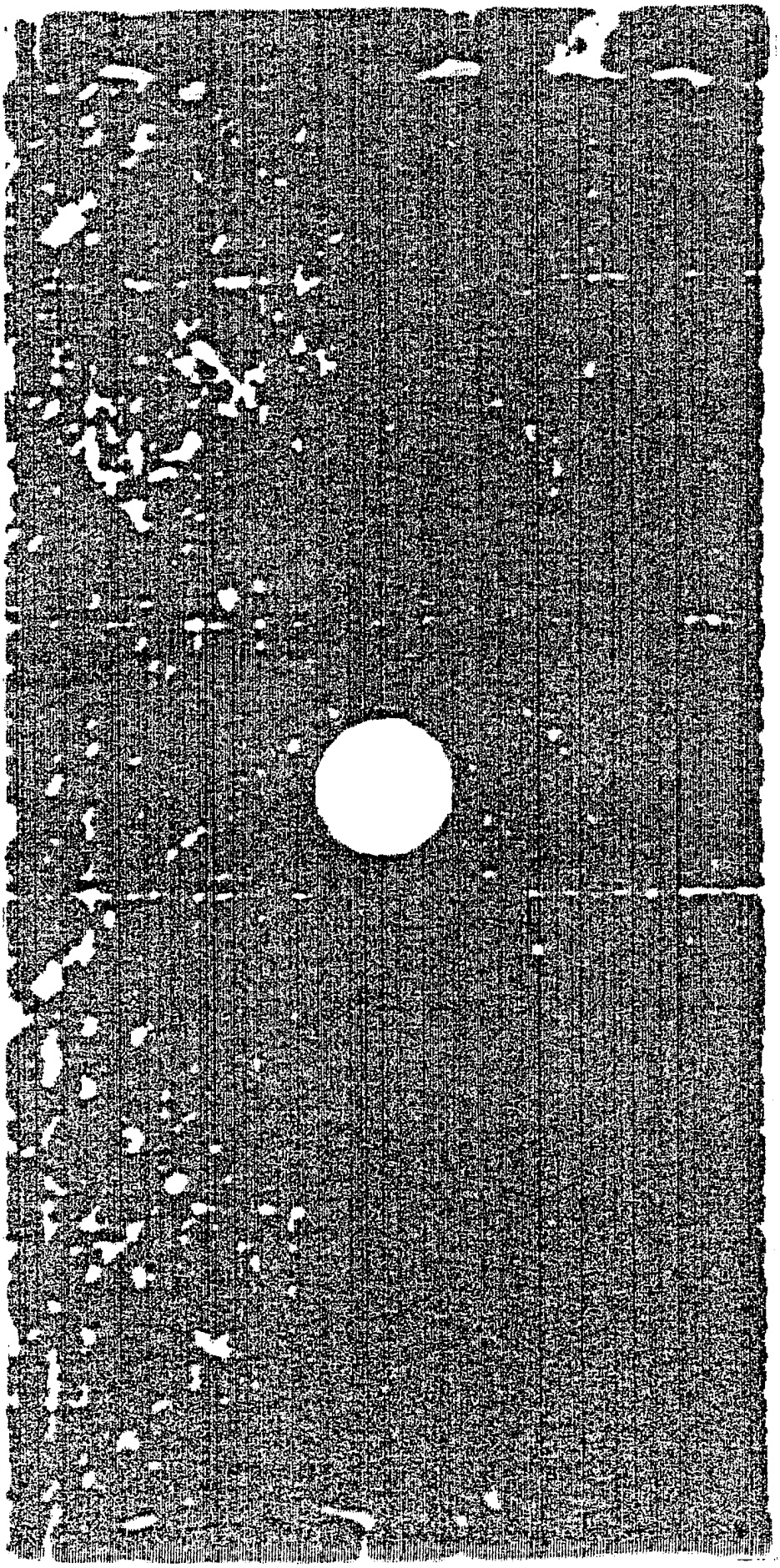

Fig. 5. Ultrasonic C-scan of the test specimen containing a 3/4 inch hole.

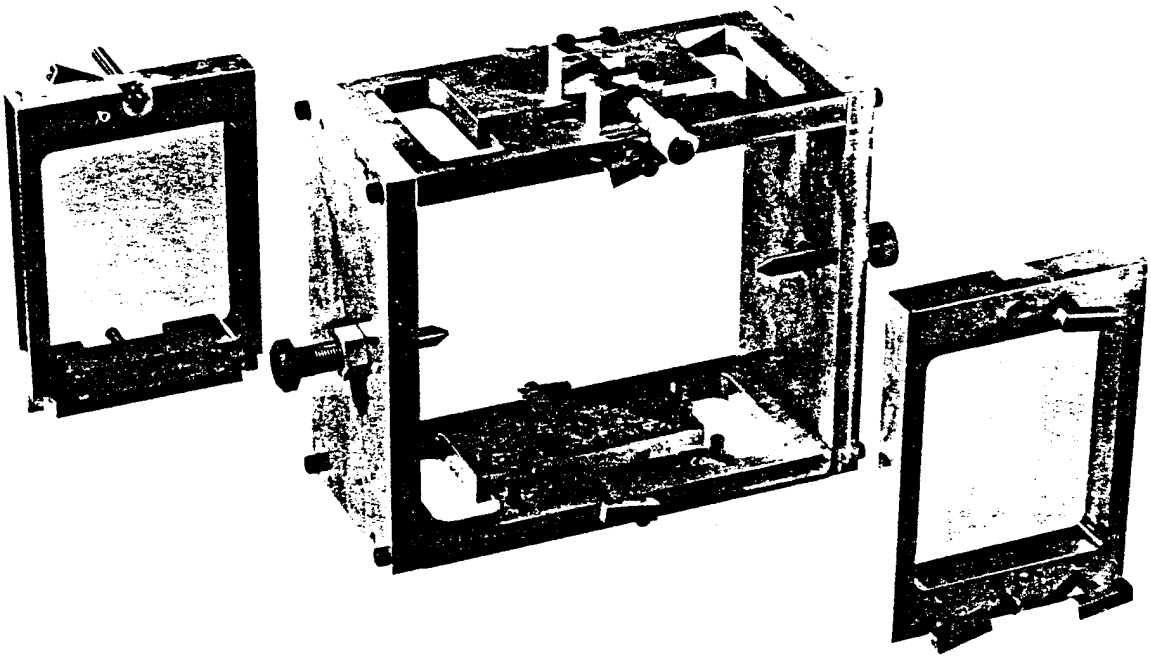

Fig. 6. Fixture for Reflection Holography. The box-like fixture attaches to the specimen and pivots about its y-axis; the micrometer adjusts inclination of the fixture. Conical seats are cemented to the specimen to prevent damage by the pivot points. Photographic plates are clipped onto each frame and subsequently inserted into the fixture.

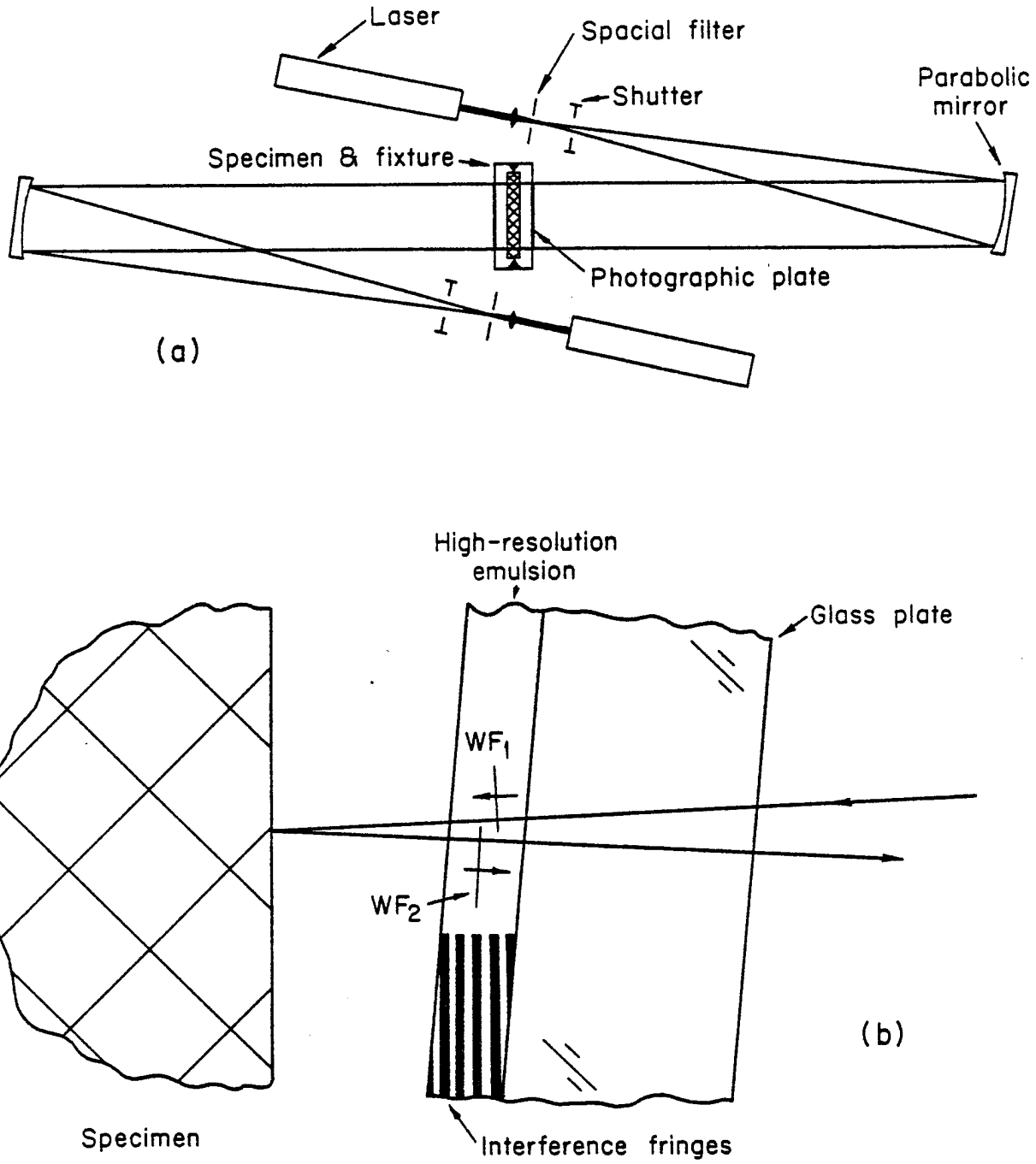

Fig. 7. (a) Optical system for the holographic exposures. (b) The incoming (reference) beam and reflected (information) beam form a stationary pattern of constructive and destructive interference in the volume of the photographic emulsion.

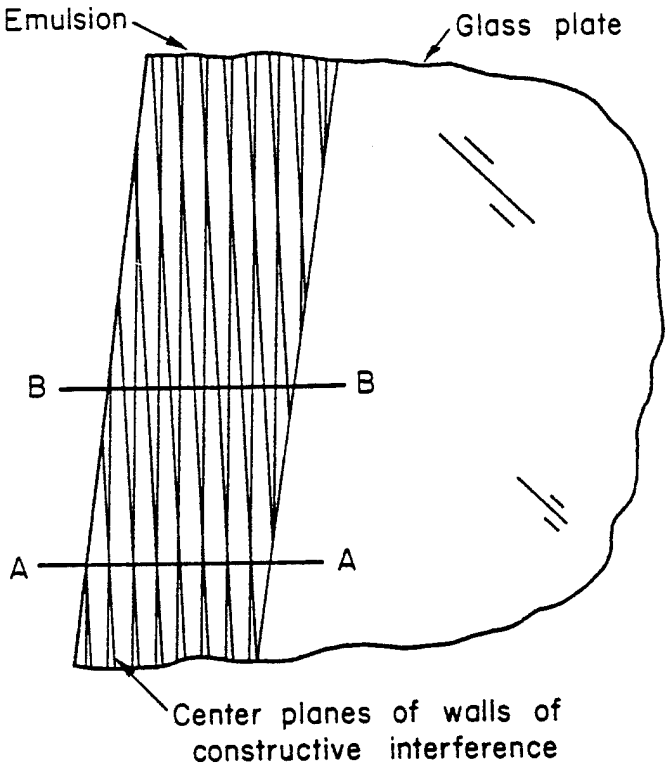

Fig. 8. Each doubly-exposed photographic plate captures two systems of interference fringes, representing specimen surface warpage before and after the load increment, respectively.

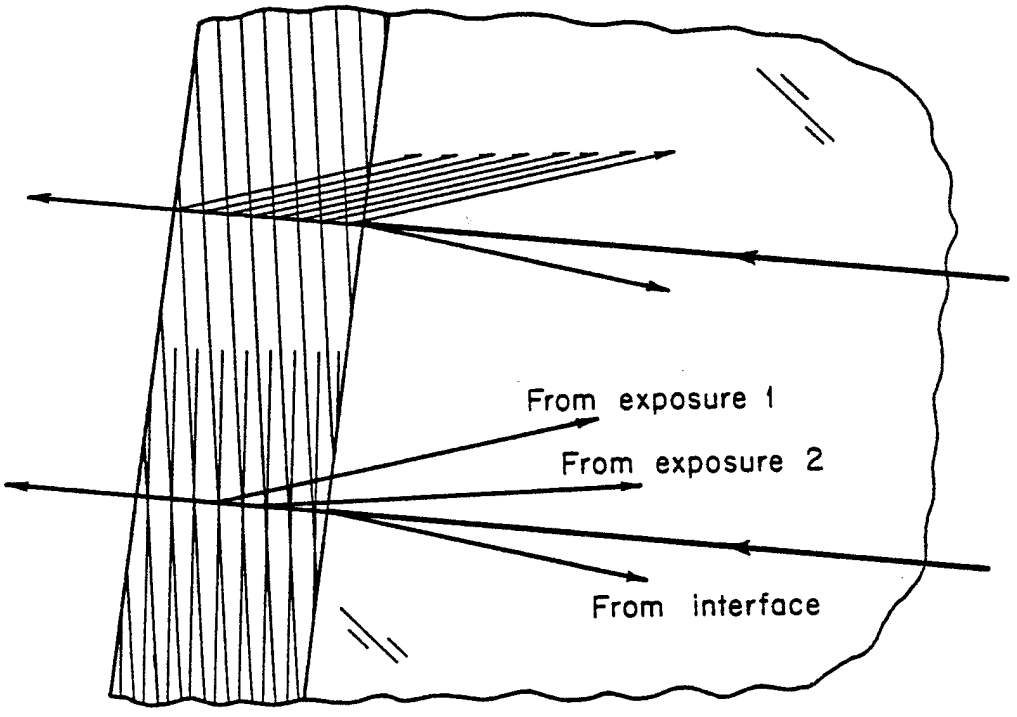

Fig. 9. After development, the walls of constructive interference become partial mirrors and reflect light in the direction taken by the information beam at the time of the holographic exposure.

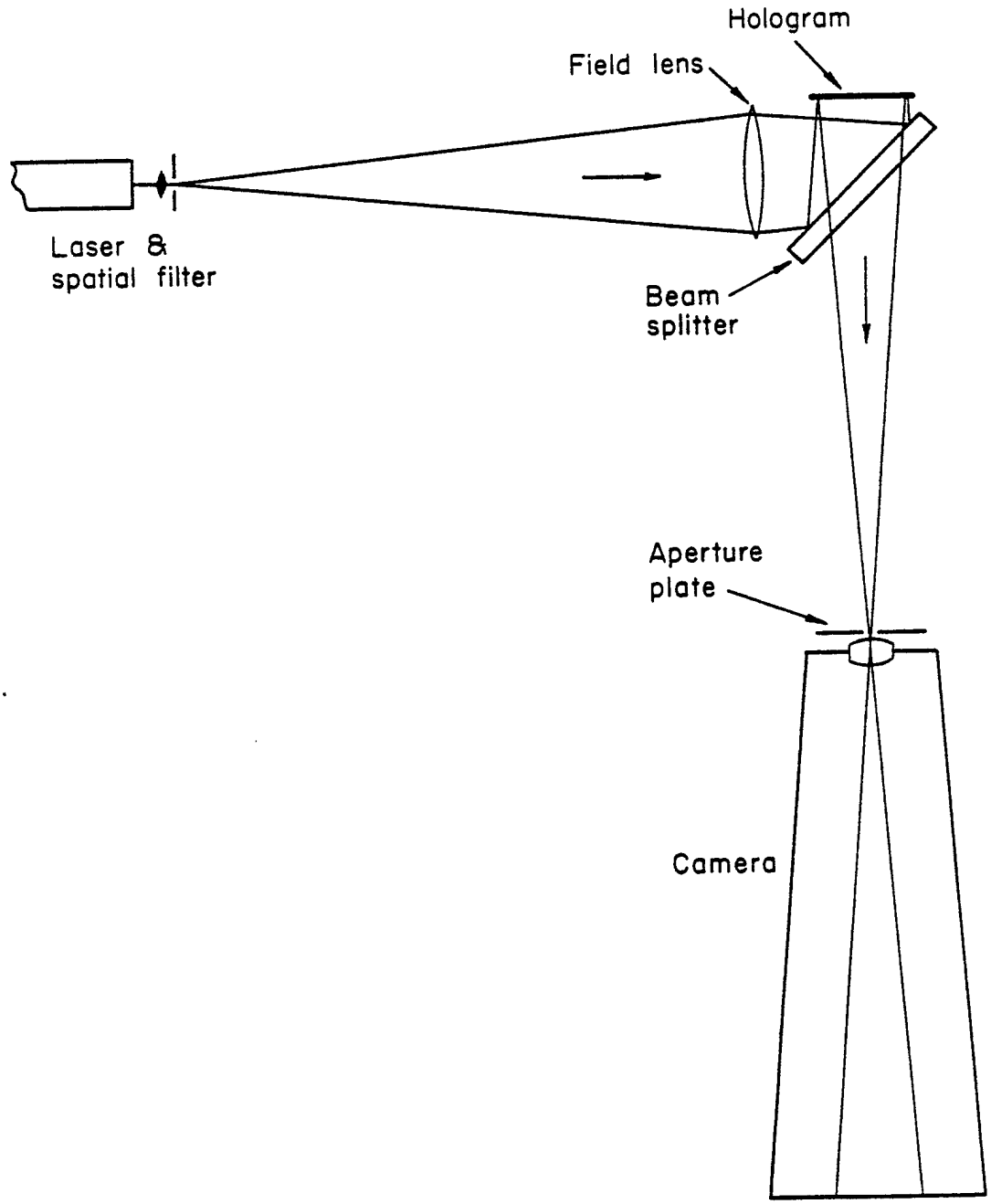

Fig. 10. Optical system used to reconstruct the hologram images.

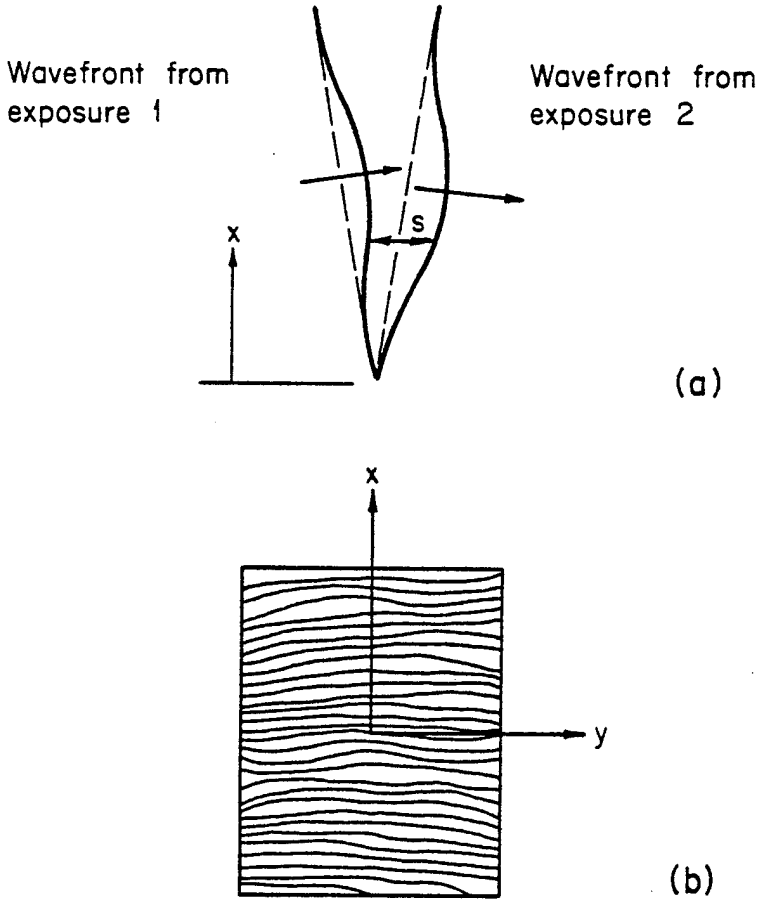

Fig. 11. (a) Upon reconstruction, wavefronts emerge from each hologram with warpage representing the specimen surface before and after the load increment; their relative inclination forms a carrier pattern. (b) They combine through optical interference to form a contour map of s, where information depicting the difference of wavefront warpages appears as disturbances in the otherwise regular carrier pattern.

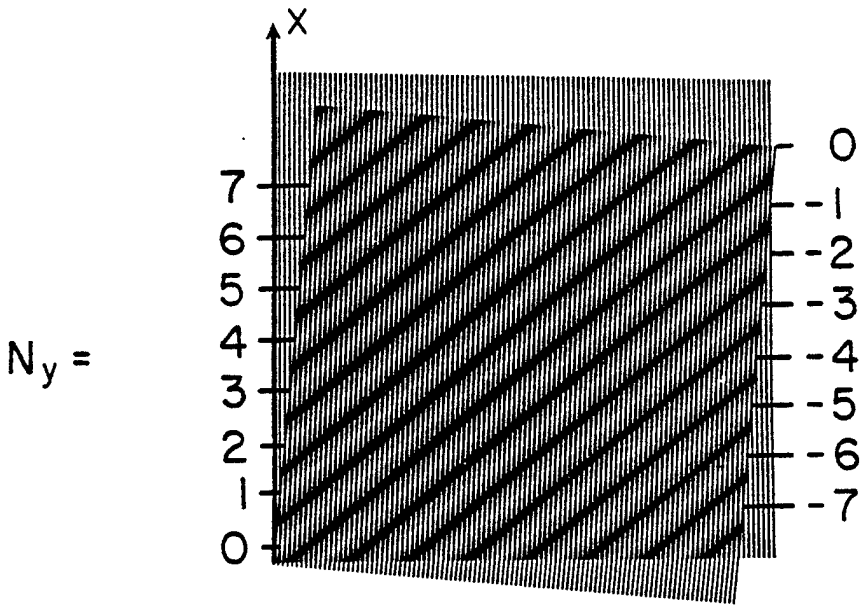

(a)

(b)

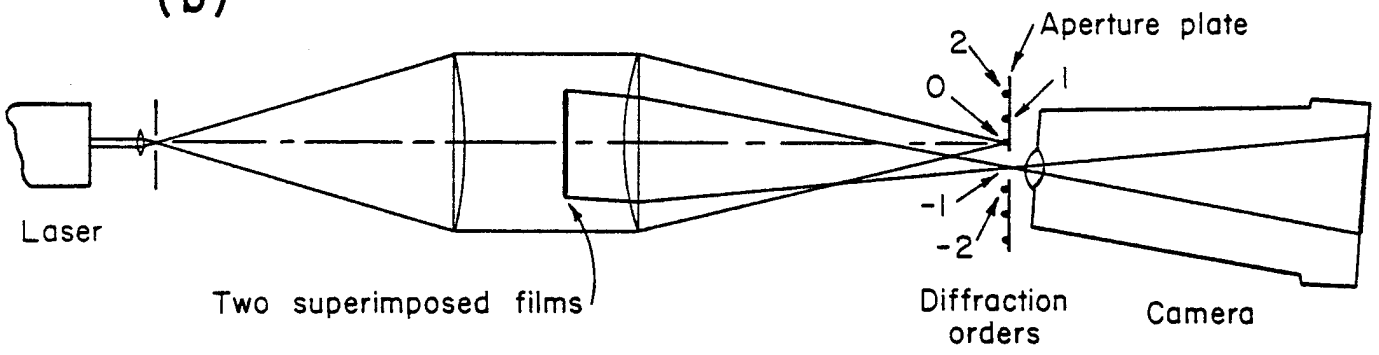

Fig. 12. (a) Superposition of the contour maps from faces I and II forms moire fringes that depict changes of specimen thickness. (b) Arrangement for optical filtering to enhance contrast of the moire fringes.

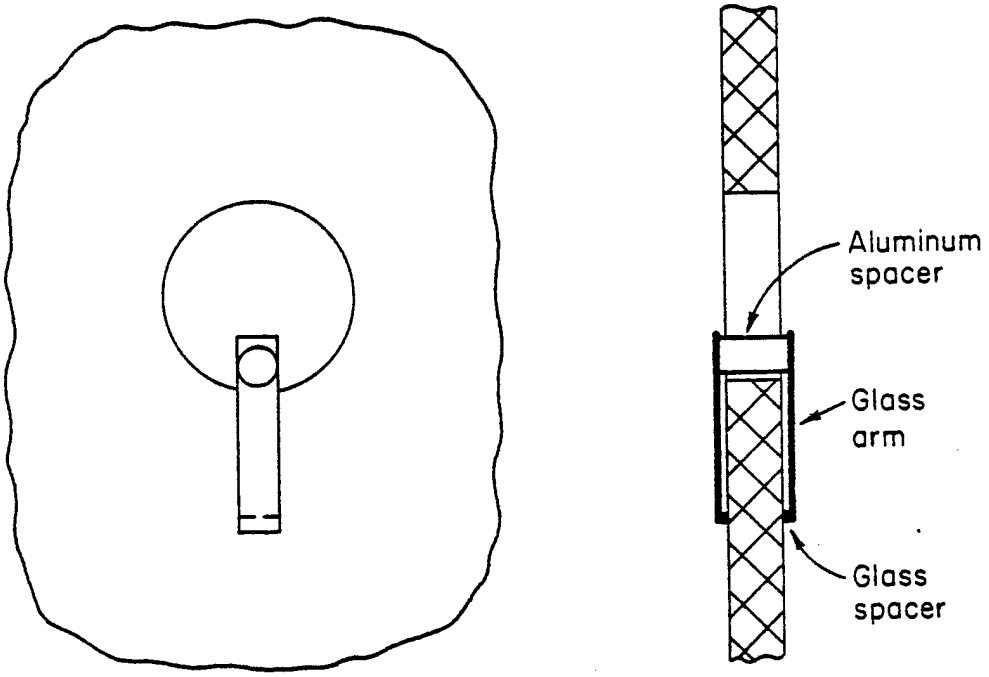

Fig. 13. Configuration and location of Clip Gage 2 used to measure the absolute change of thickness at a point in the field of view.

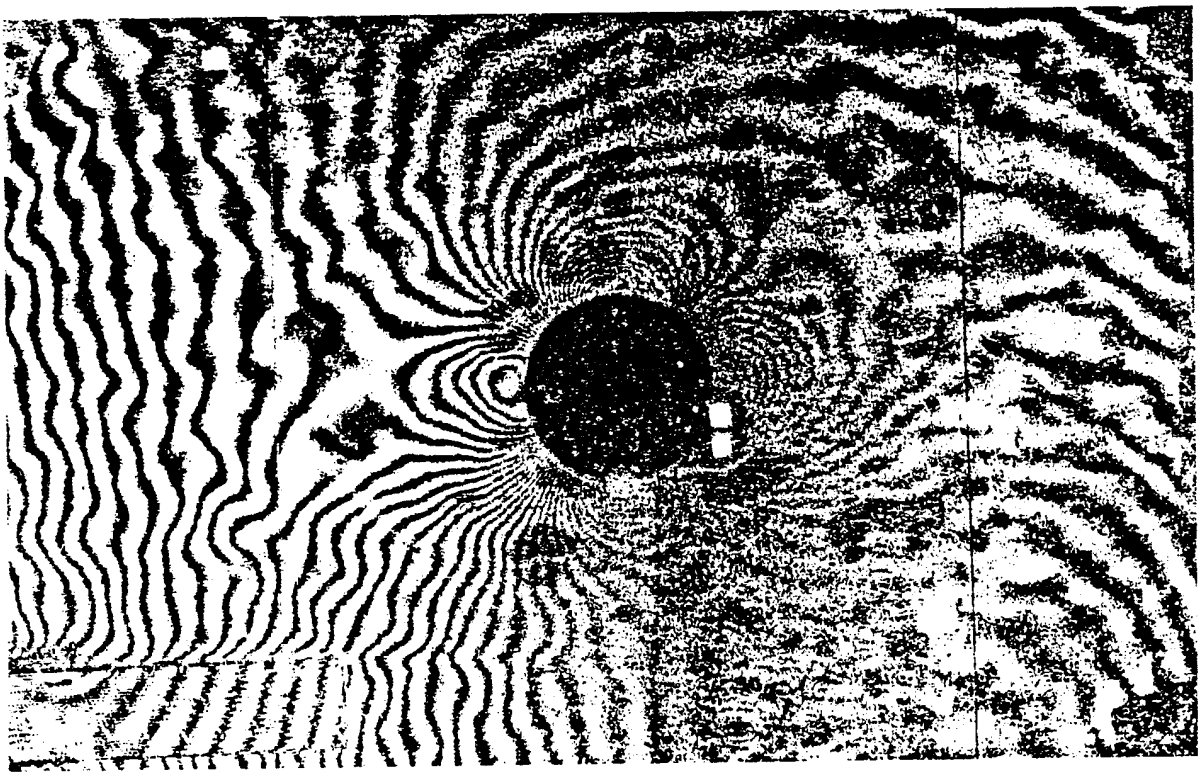

Fig. 14. Change of thickness contour maps for the test specimen containing a 1/2 inch hole. (a) Contour map for the 480-16000 lbs load increment, #1.

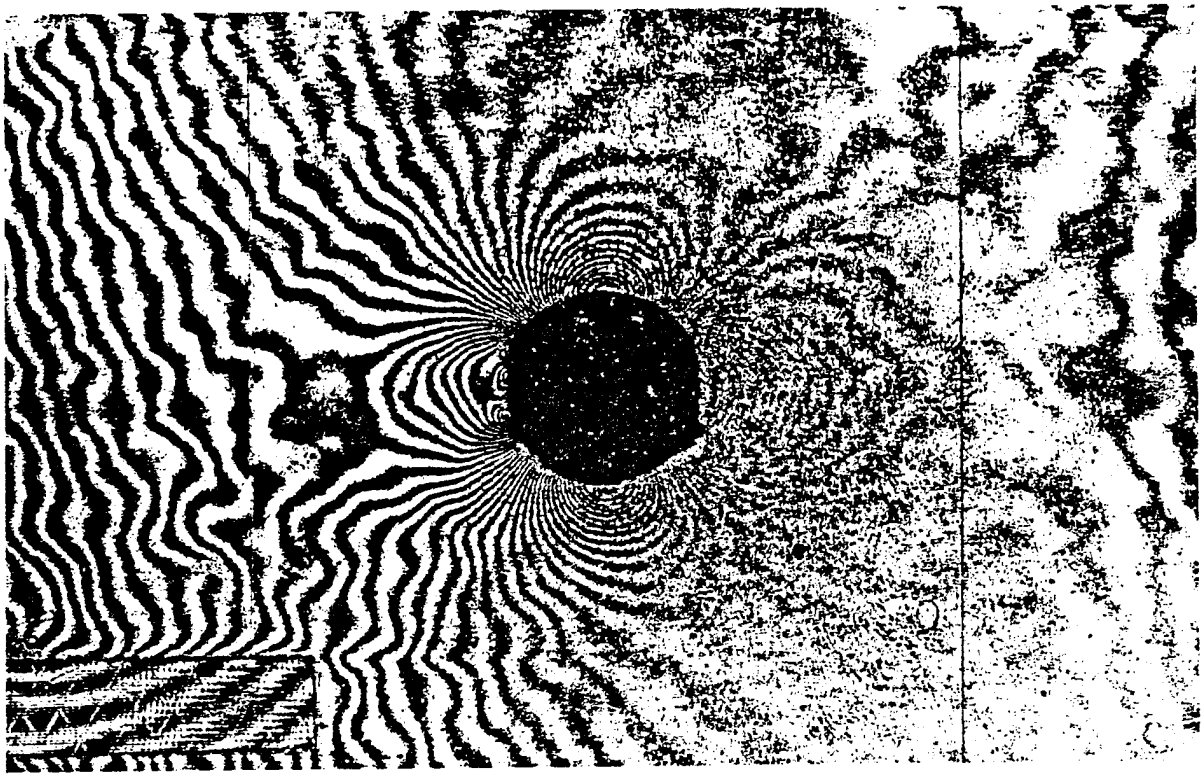

Fig. 14. (b) Contour map for the 29800-45000 lbs load increment, #3.

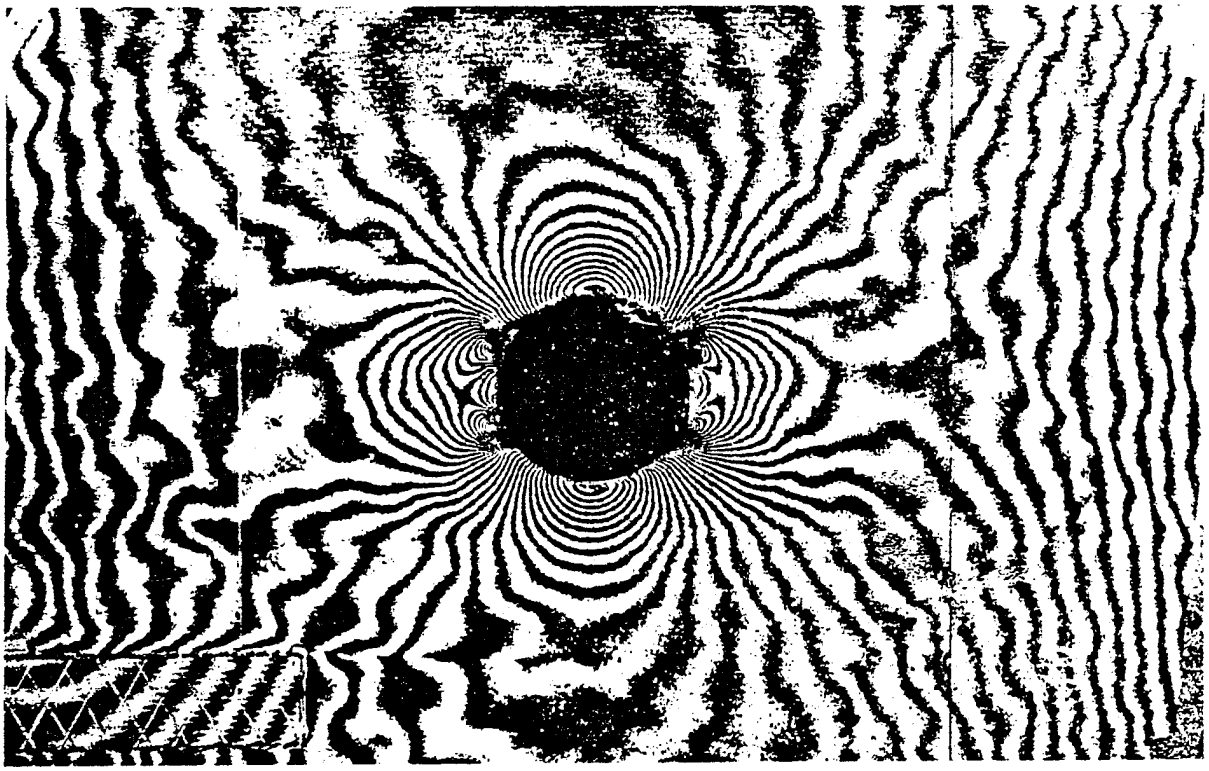

Fig. 14. (c) Contour map for the 44800-57150 lbs load increment, #4.

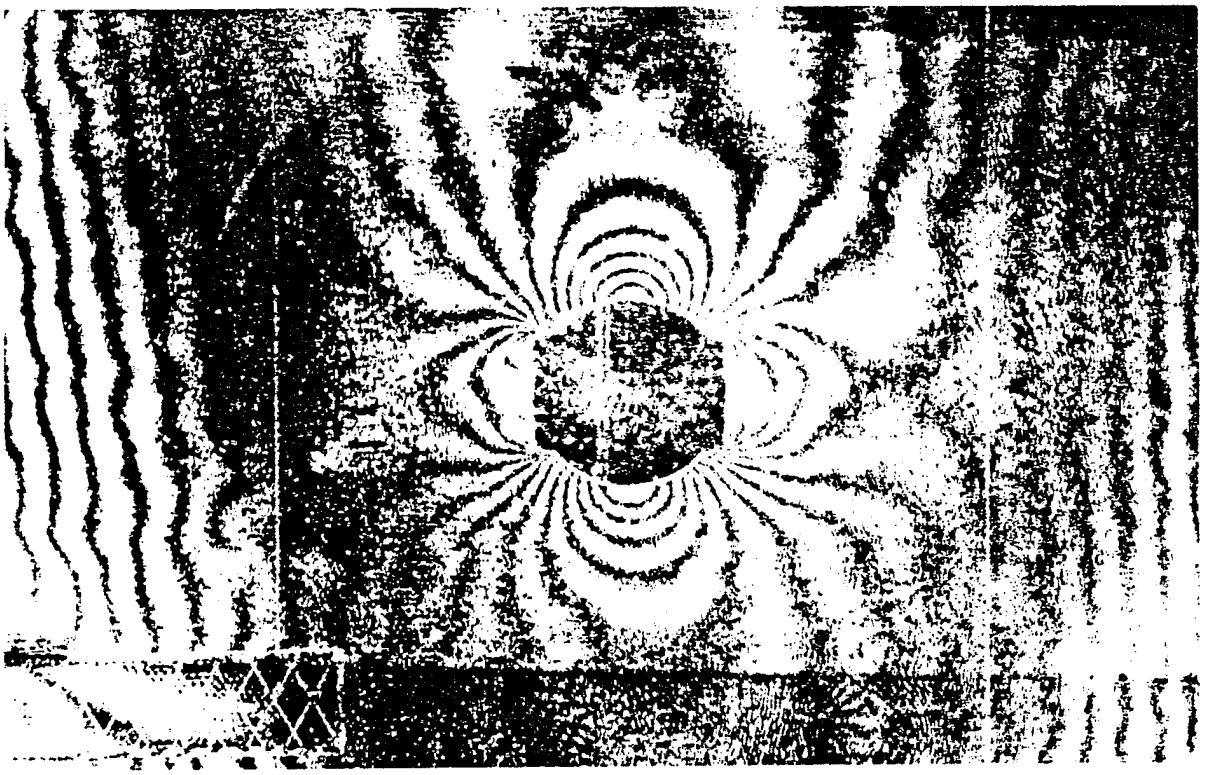

Fig. 14. (d) Contour map for the 56900-62050 lbs load increment, #5.

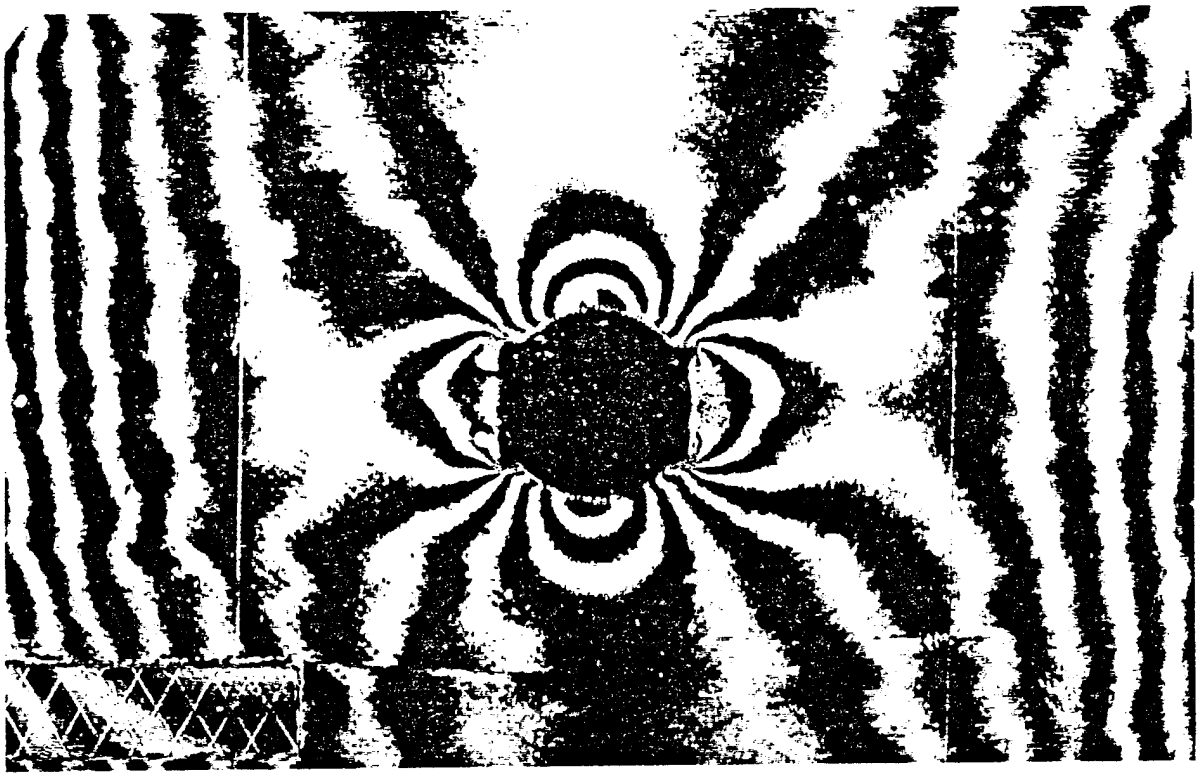

Fig. 14. (e) Contour map for the 62000-65000 lbs load increment, #6.

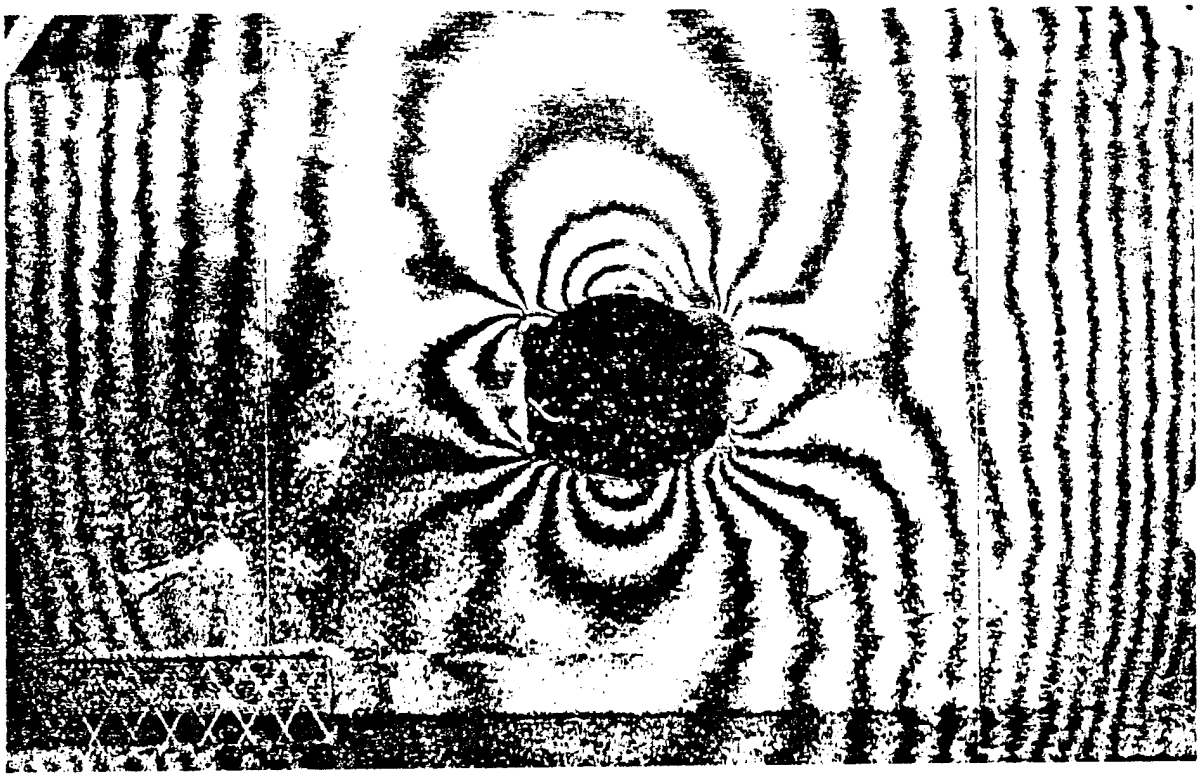

Fig. 14. (f) Contour map for the 64700-68000 lbs load increment, #7.

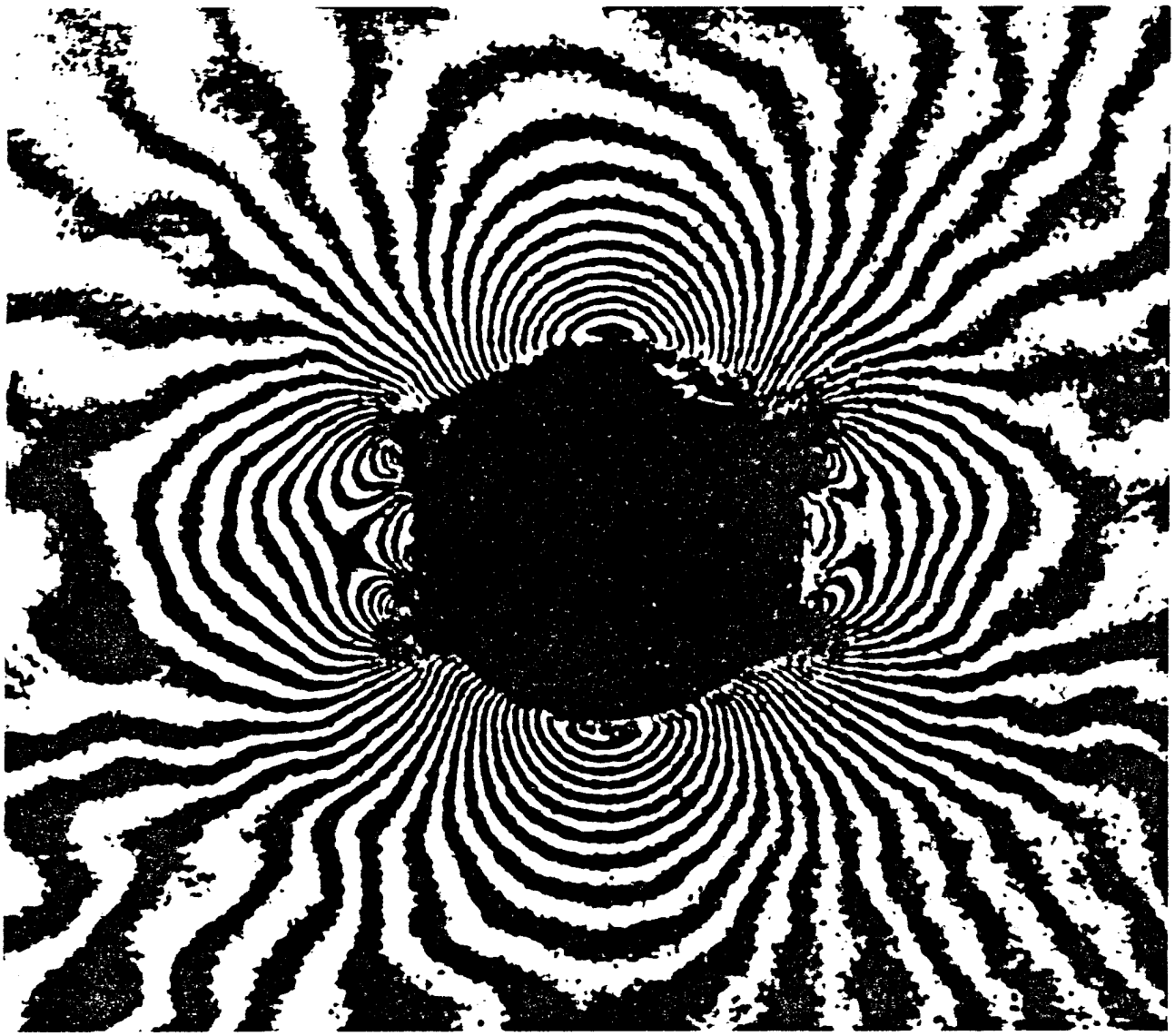

Fig. 15. Enlargement of the contour map shown in Fig. 14(c).

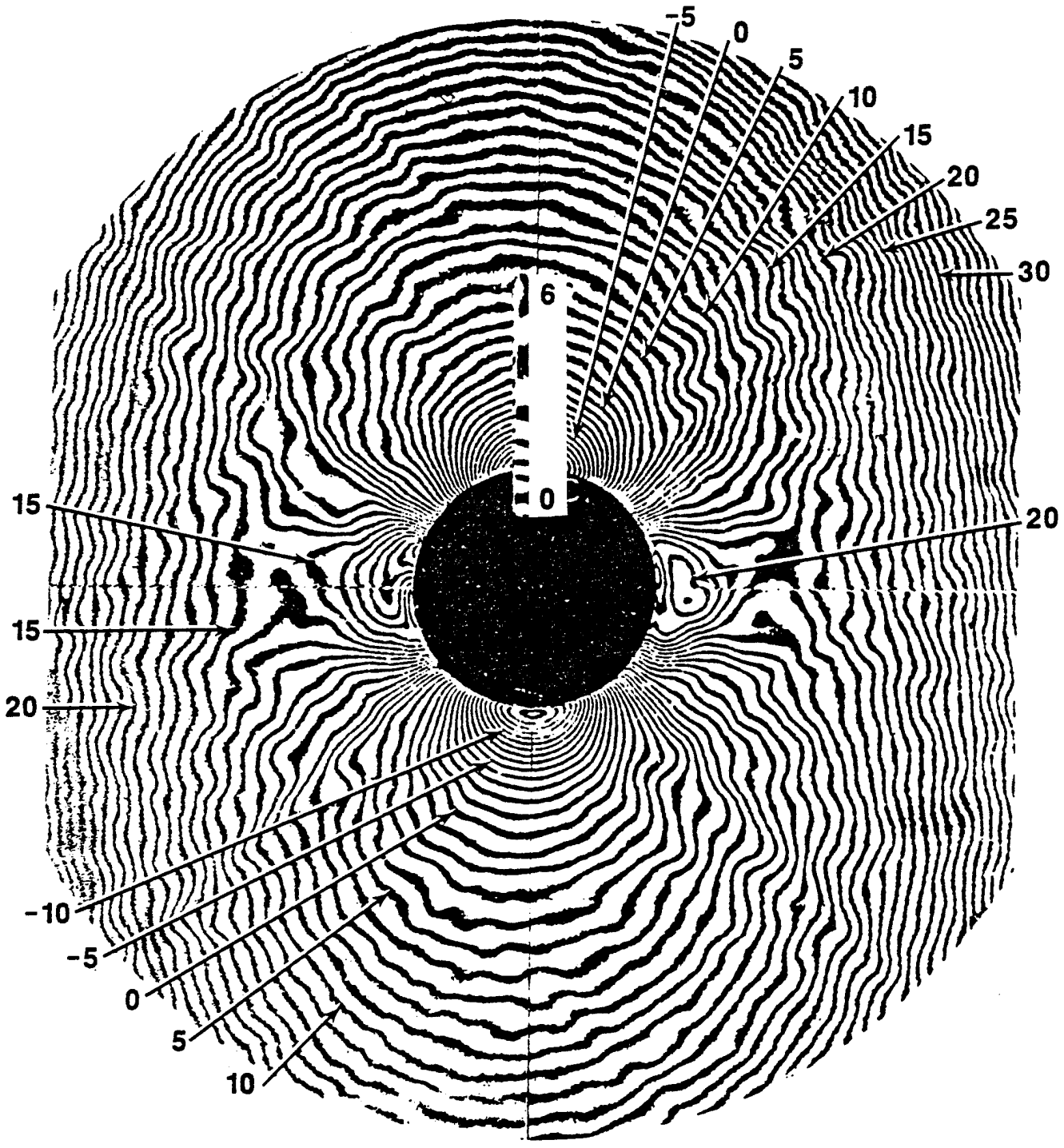

Fig. 16. Change of thickness contour maps for the test specimen containing a 3/4 inch hole. (a) Contour map for the 14900-29850 lbs load increment, #2.

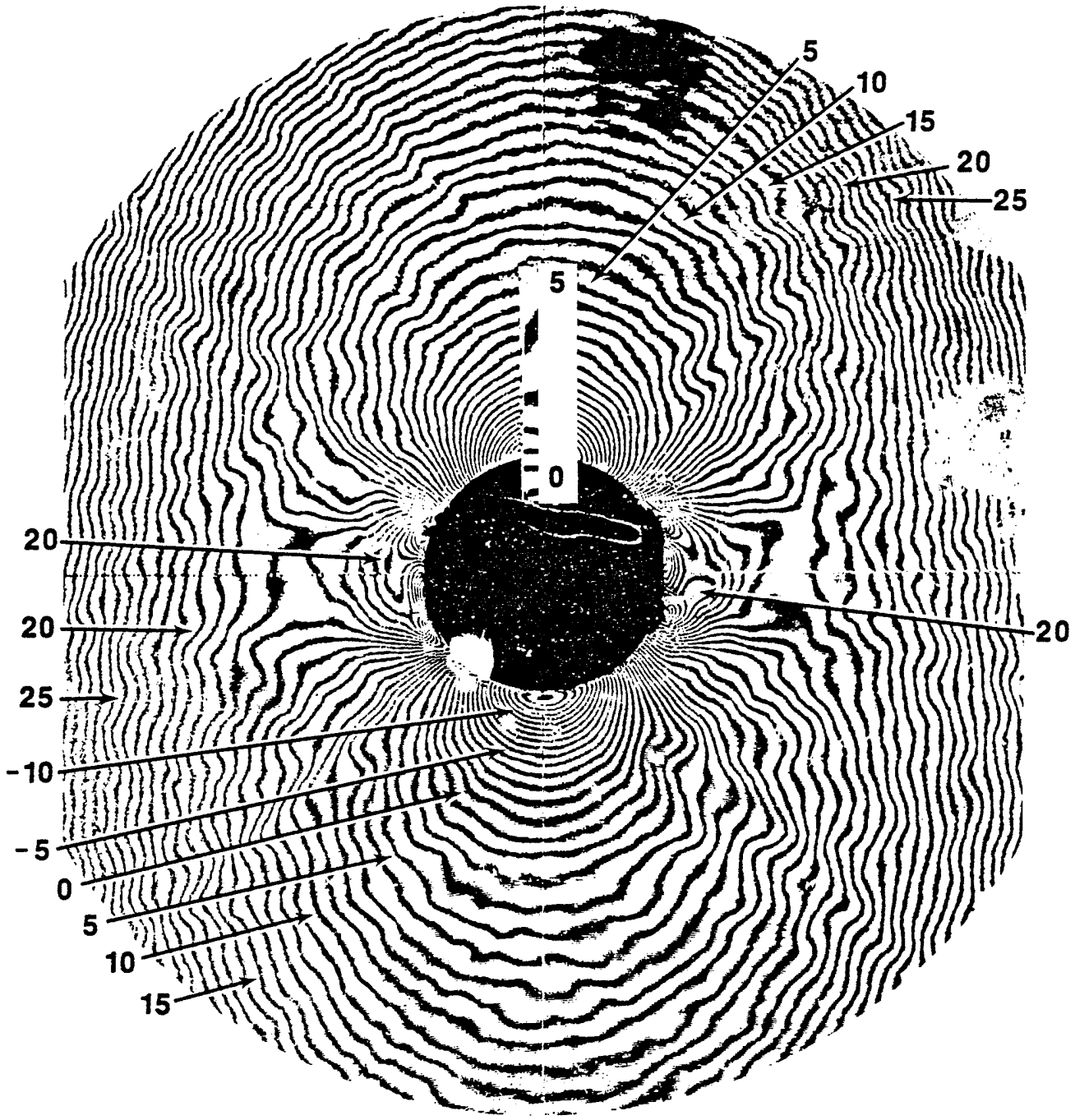

Fig. 16. (b) Contour map for the 29850-44650 lbs load increment, #3.

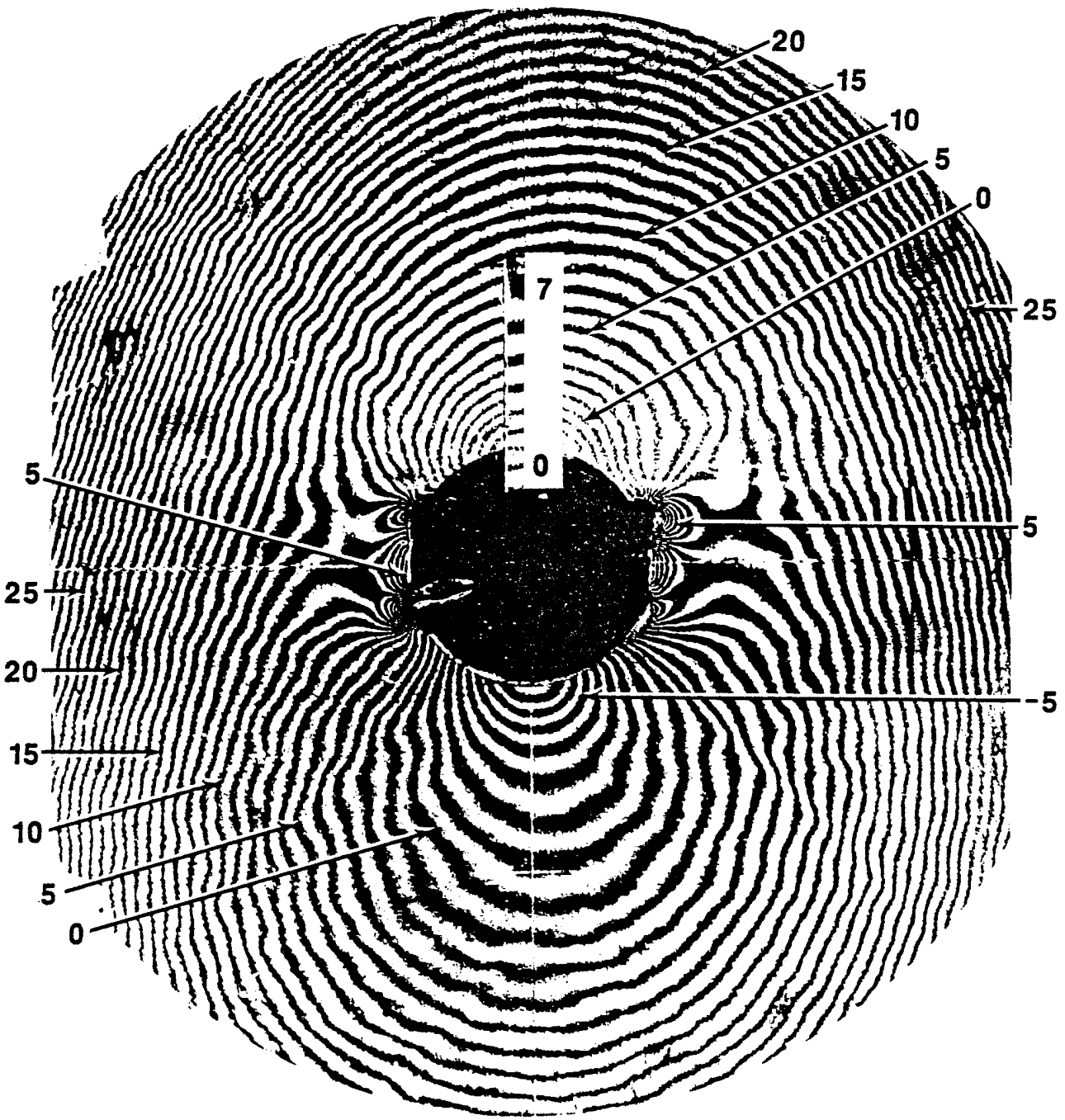

Fig. 16. (c) Contour map for the 44550-49925 lbs load increment, #4.

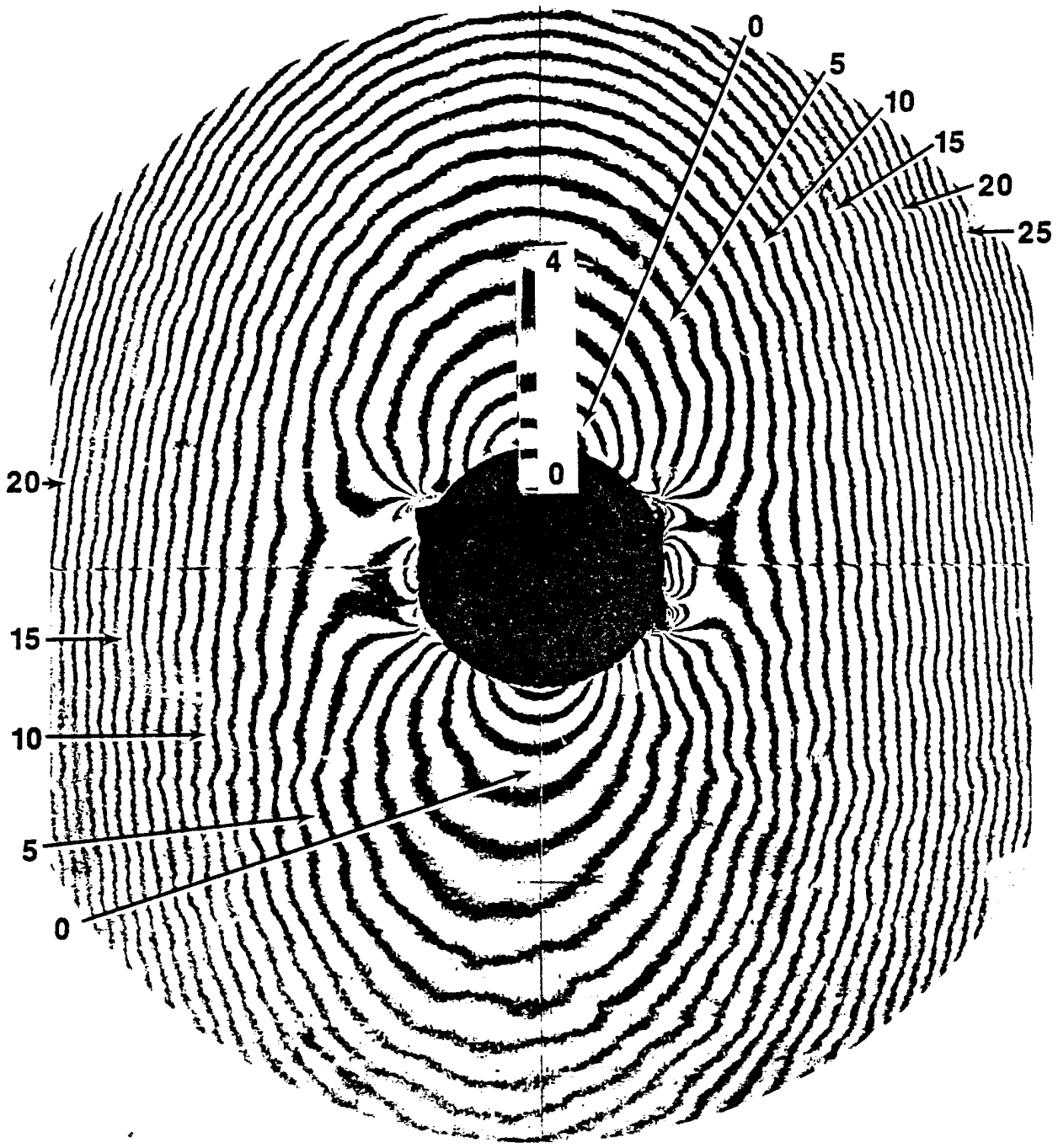

Fig. 16. (d) Contour map for the 49925-52750 lbs load increment, #5.

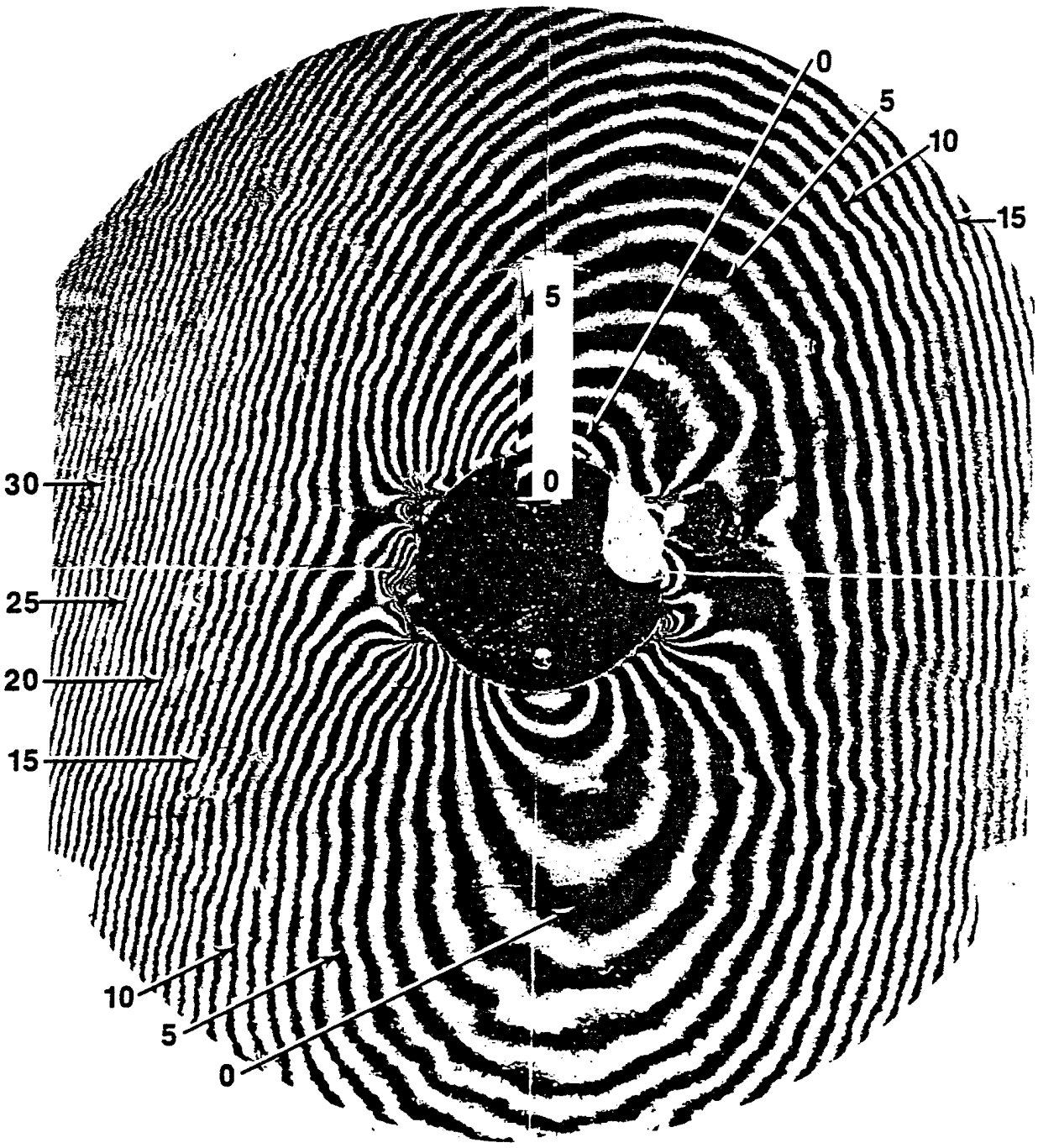

Fig. 16. (e) Contour map for the 52750-55800 lbs load increment, #6.

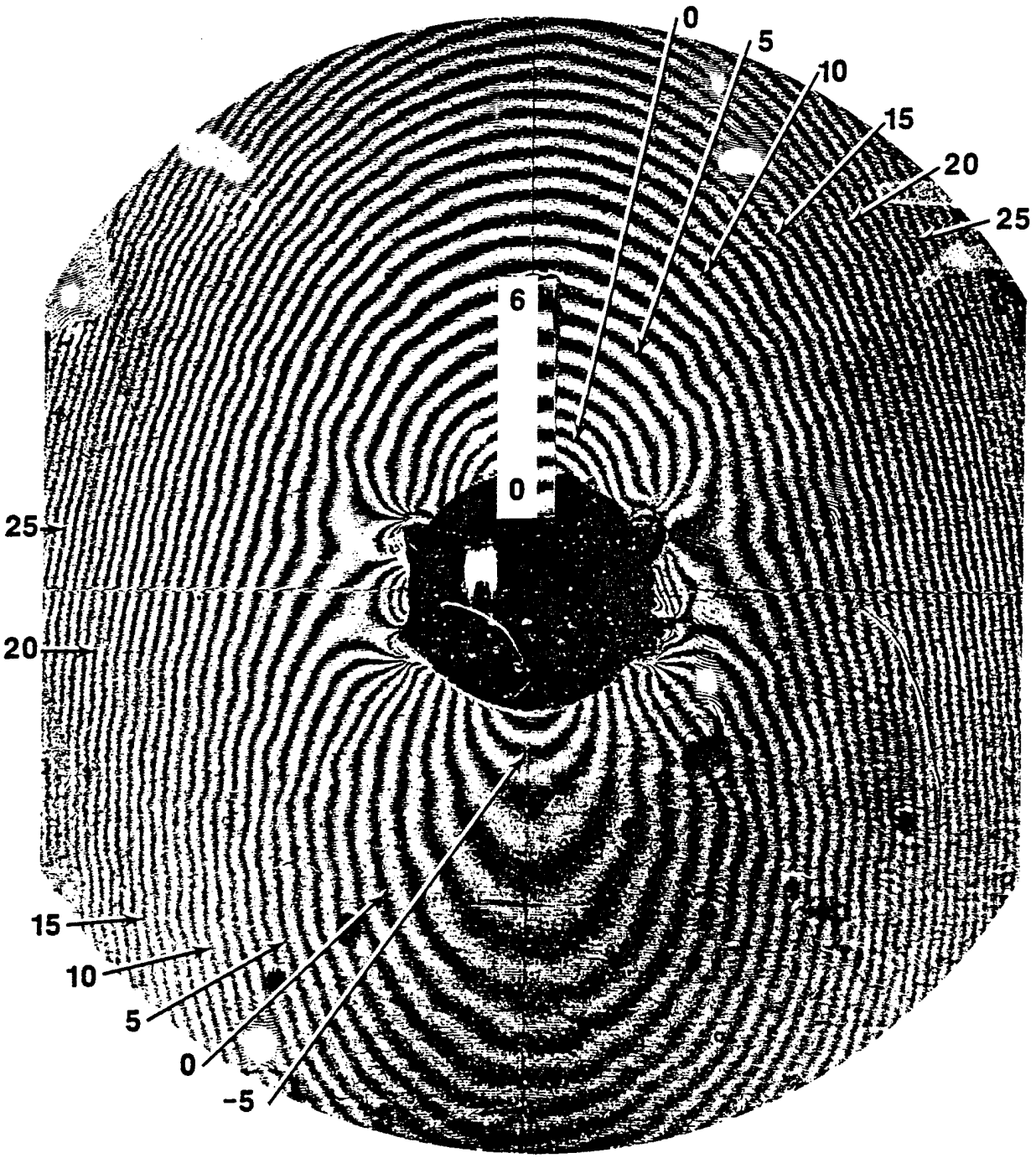

Fig. 16. (f) Contour map for the 55800-58850 lbs load increment, #7.

Fig. 17. Enlargement of the contour map shown in Fig. 16(a).

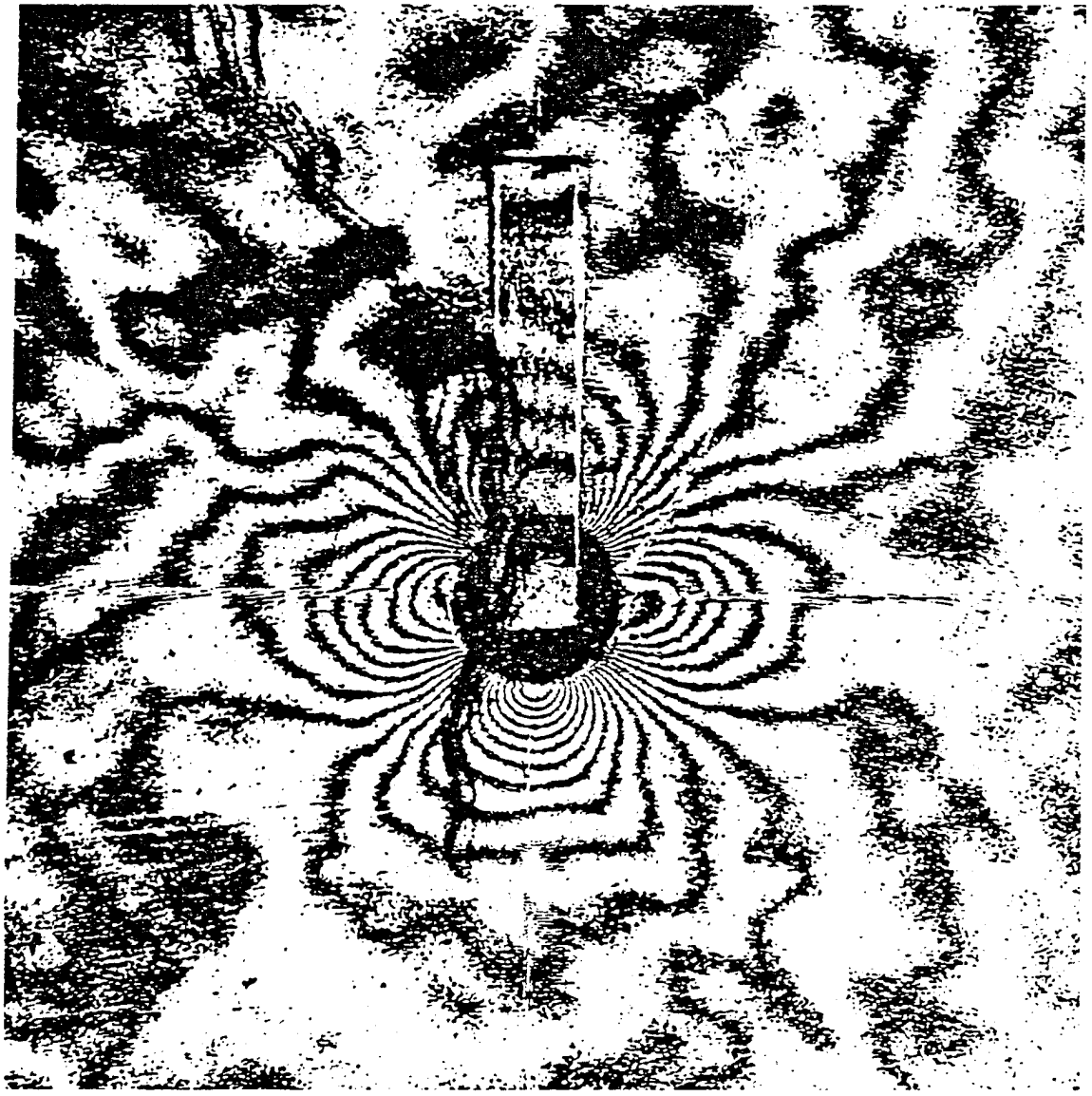

Fig. 18. Change of thickness contour maps in the vicinity of the hole for the test specimen containing a 1/4 inch hole. (a) Contour map for the 550-14800 lbs load increment, #1.

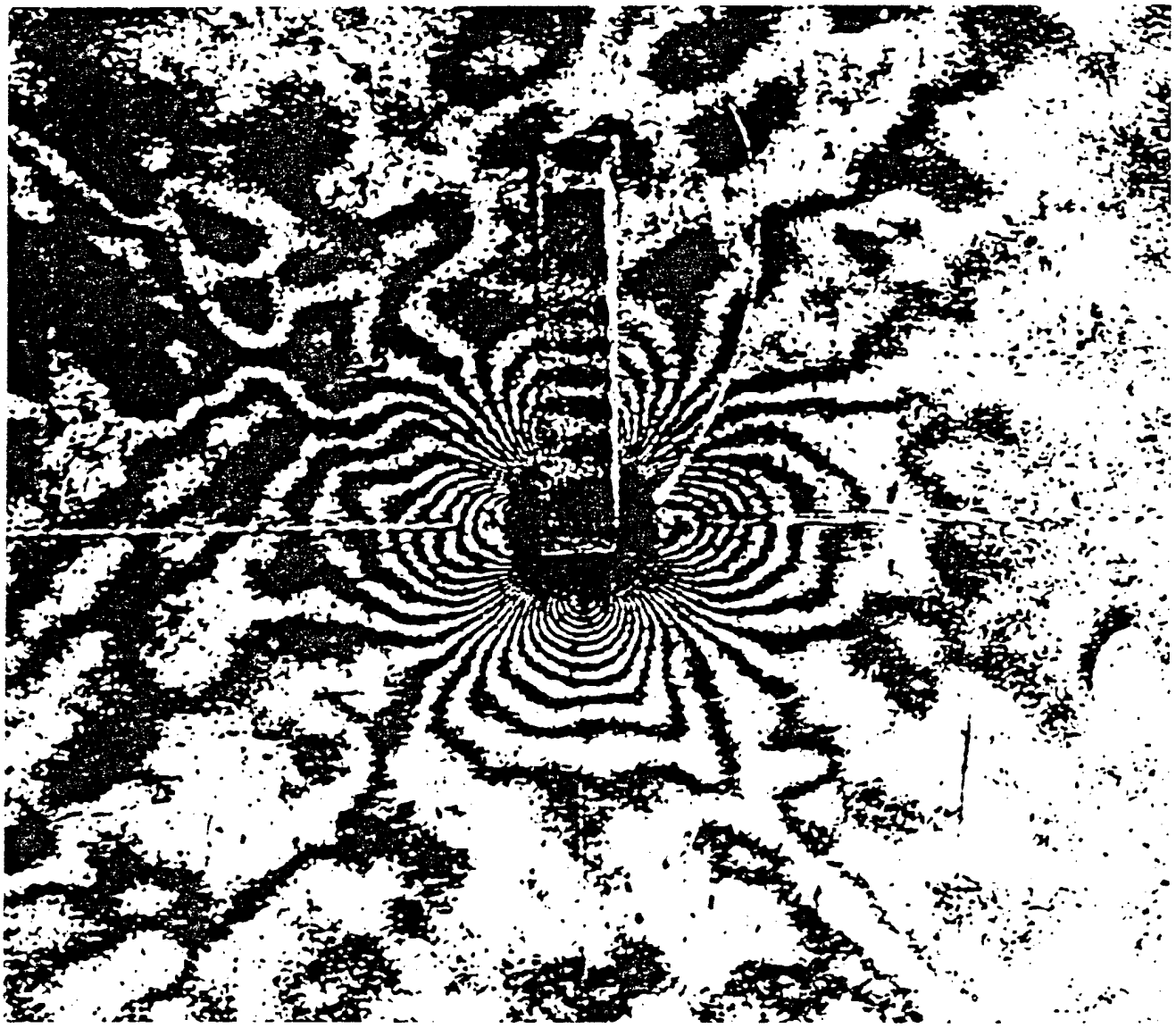

Fig. 18. (b) Contour map for the 14800-29650 lbs load increment, #2.

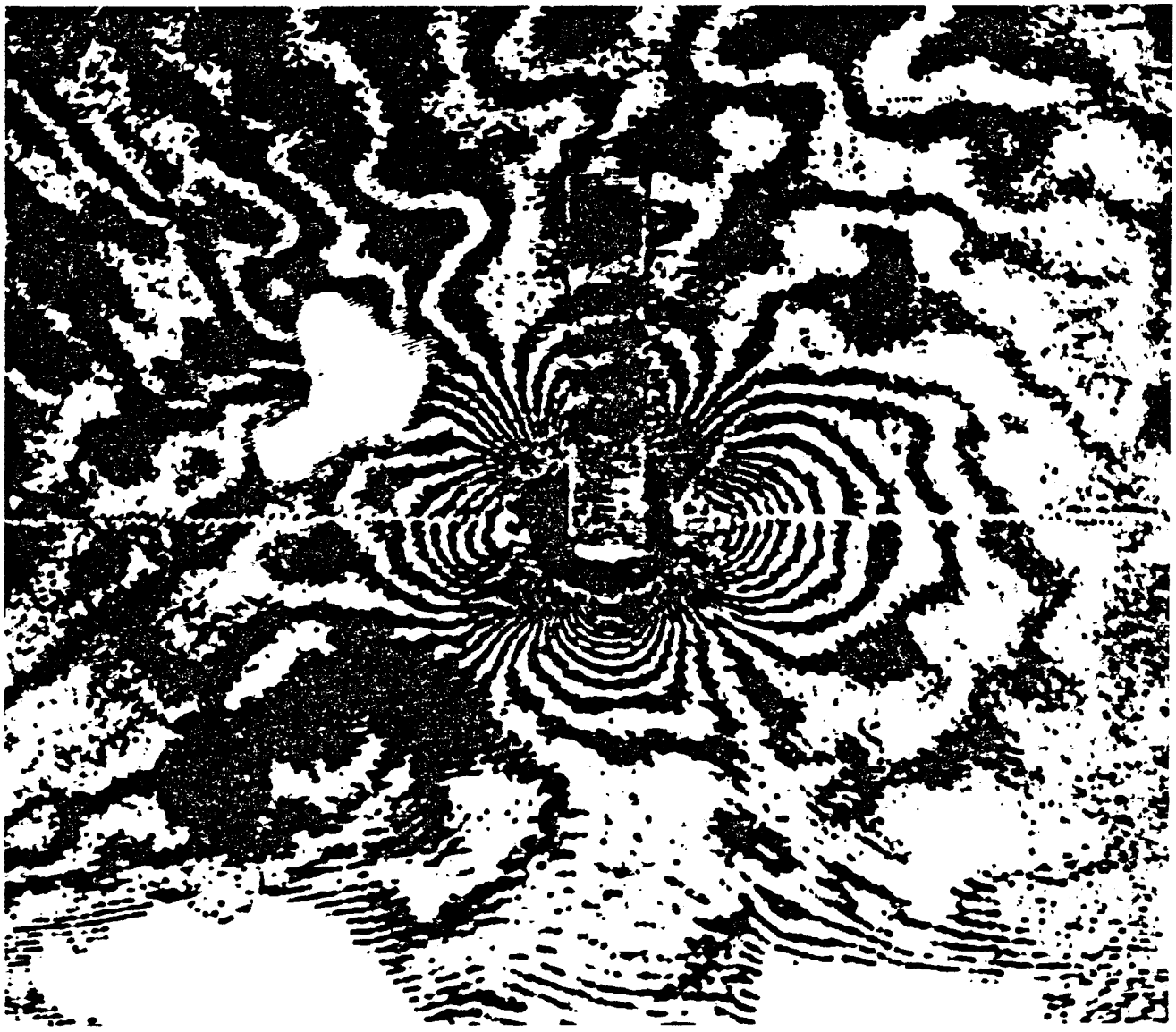

Fig. 18. (c) Contour map for the 45250-59400 lbs load increment, #4.

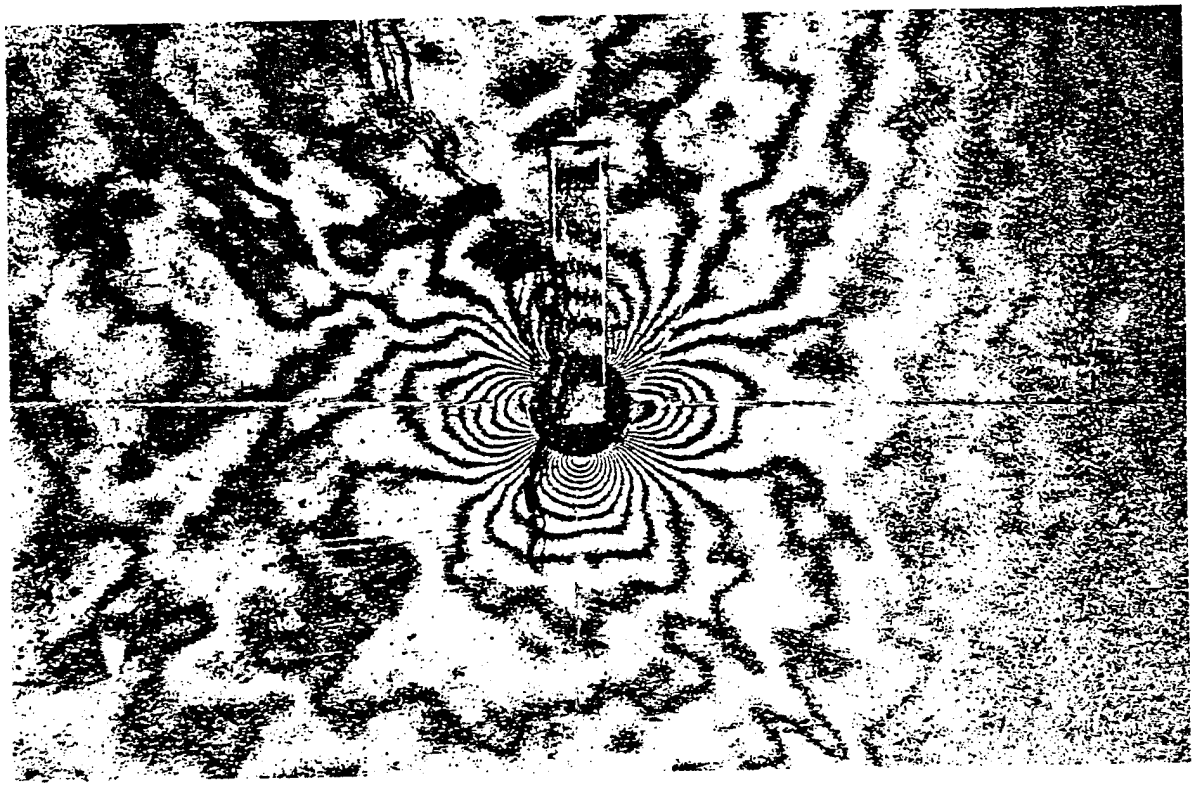

Fig. 19. Contour map corresponding to Fig. 18 (a) showing a large field of view.

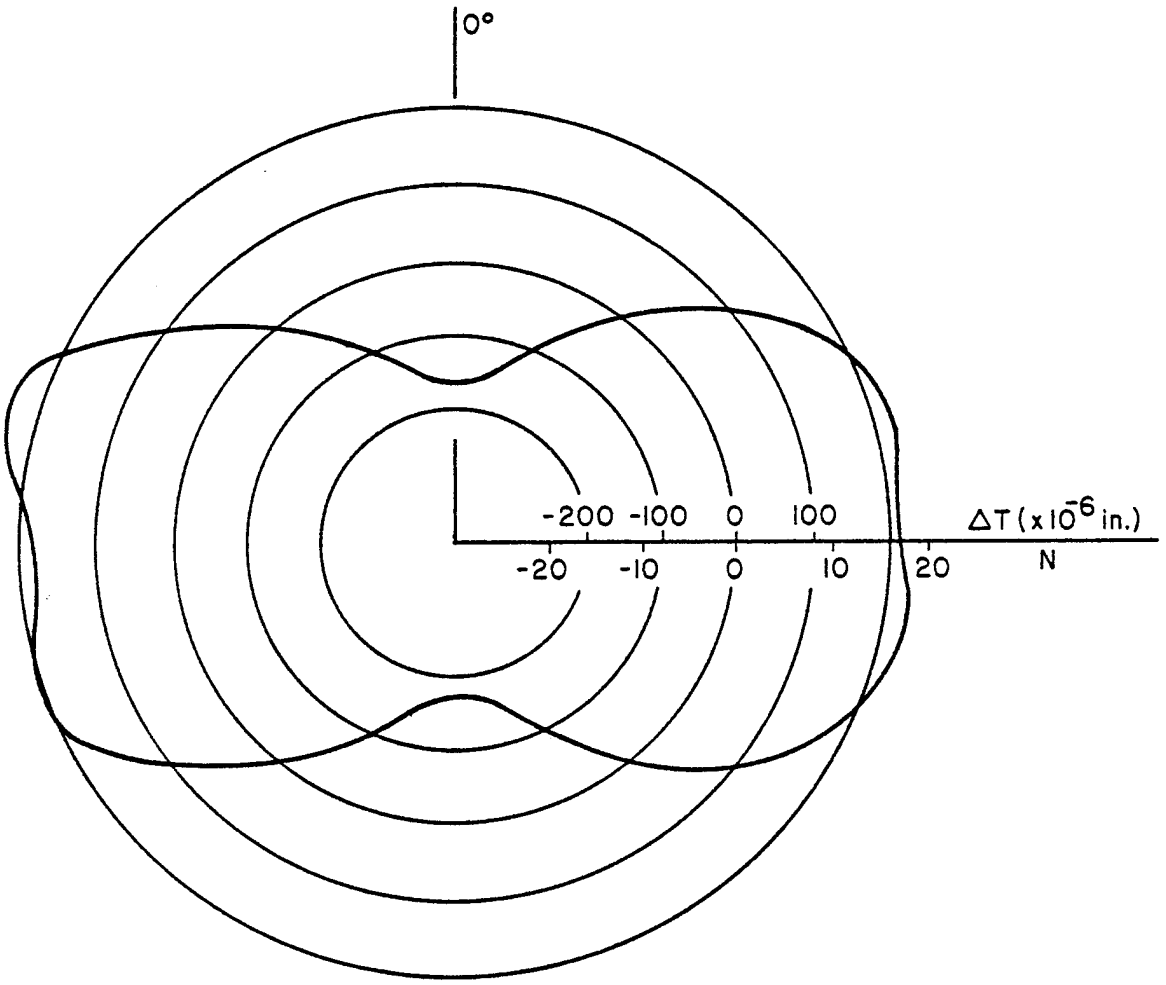

Fig. 20. Polar plot of the change of thickness along the boundary of the 3/4 inch hole which resulted from the second increment of load. The contour map shown in Fig. 17. was used to make this plot.

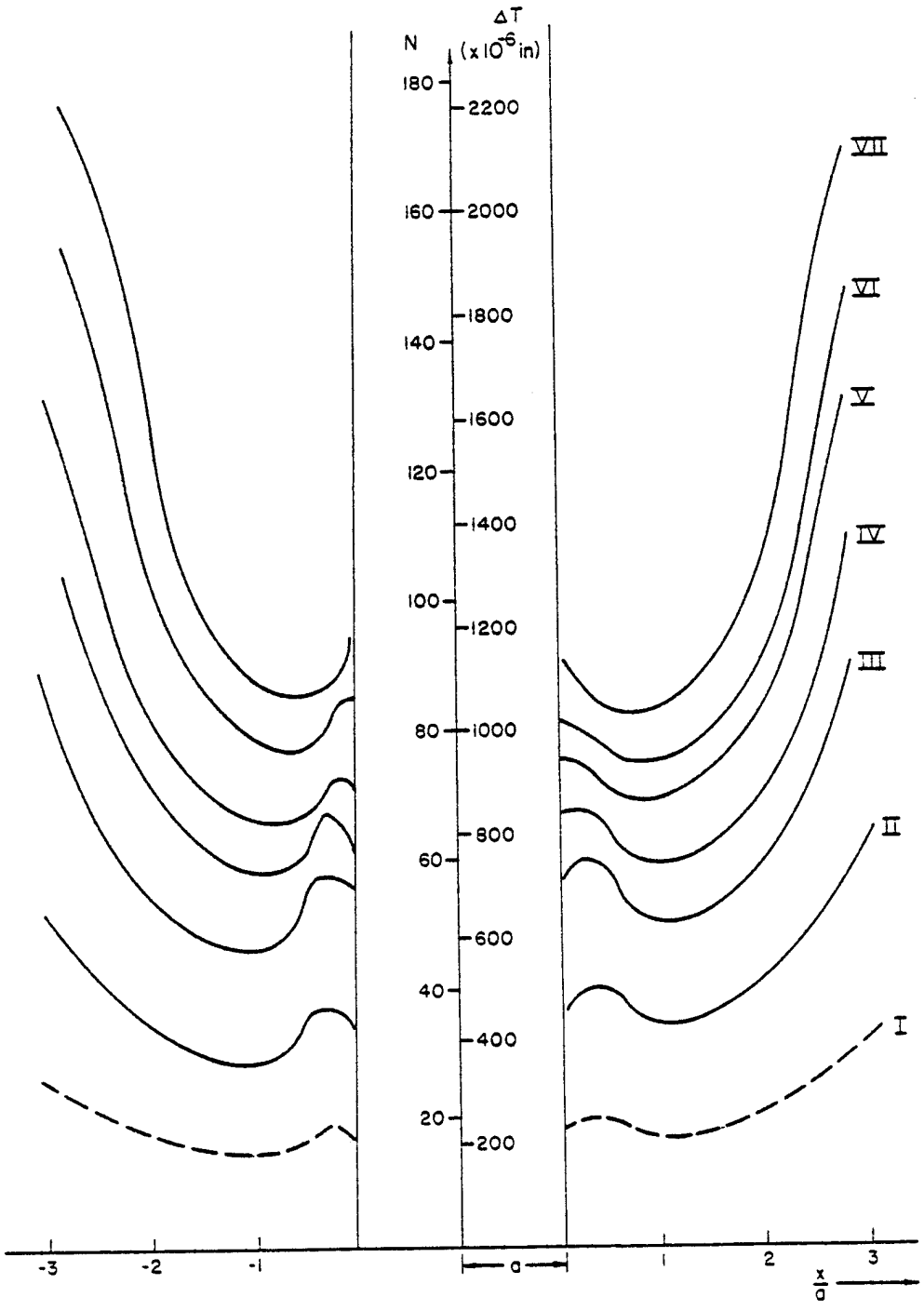

Fig. 21. Thickness change versus position on the horizontal centerline for various load levels: I-14925 lbs, II-29850 lbs, III-44650 lbs, IV-49925 lbs, V-52750 lbs, VI-55800 lbs, VII-58850 lbs. The dashed curve, graph I, is an approximation taken as equal to ΔT for the load increment I to II.